Earth Syst. Dynam. Discuss., 5, 203–279, 2014
www.earth-syst-dynam-discuss.net/5/203/2014/
doi:10.5194/esdd-5-203-2014

Earth System Dynamics Discussions
Open Access

Contrasting roles of interception and transpiration in the hydrological cycle – Part 1: Simple Terrestrial Evaporation to Atmosphere Model

L. Wang-Erlandsson[1,2], R. J. van der Ent[1], L. J. Gordon[2], and H. H. G. Savenije[1]

[1]Department of Water Management, Faculty of Civil Engineering and Geosciences, Delft University of Technology, Delft, the Netherlands
[2]Stockholm Resilience Centre, Stockholm University, Stockholm, Sweden

Received: 25 February 2014 – Accepted: 4 March 2014 – Published: 14 March 2014

Correspondence to: L. Wang-Erlandsson (l.wang-2@tudelft.nl)

Published by Copernicus Publications on behalf of the European Geosciences Union.

Abstract

Terrestrial evaporation consists of biophysical (i.e., transpiration) and physical fluxes (i.e., interception, soil moisture, and open water). The partitioning between them depends on both climate and the land surface, and determines the time scale of evaporation. However, few land-surface models have analysed and evaluated evaporative partitioning based on land use, and no studies have examined their subsequent paths in the atmosphere. This paper constitutes the first of two companion papers that investigate the contrasting effects of interception and transpiration in the hydrological cycle. Here, we present STEAM (Simple Terrestrial Evaporation to Atmosphere Model) used to produce partitioned evaporation and analyse the characteristics of different evaporation fluxes on land. STEAM represents 19 land-use types (including irrigated land) at sub-grid level with a limited set of parameters, and includes phenology and stress functions to respond to changes in climate conditions. Using ERA-Interim reanalysis forcing for the years 1999–2008, STEAM estimates a mean global terrestrial evaporation of 73 800 km^3 $year^{-1}$, with a transpiration ratio of 59 %. We show that the terrestrial residence time scale of transpiration (days to months) has larger inter-seasonal variation and is substantially longer than that of interception (hours). Furthermore, results from an offline land-use change experiment illustrate that land-use change may lead to significant changes in evaporative partitioning even when total evaporation remains similar. In agreement with previous research, our simulations suggest that the vegetation's ability to transpire by retaining and accessing soil moisture at greater depth is critical for sustained evaporation during the dry season. Despite a relatively simple model structure, validation shows that STEAM produces realistic evaporative partitioning and hydrological fluxes that compare well with other global estimates over different locations, seasons and land-use types. We conclude that the simulated evaporation partitioning by STEAM is useful for understanding the links between land use and water resources, and can with benefit be employed for atmospheric moisture tracking.

ESDD
5, 203–279, 2014

Interception and transpiration – Part 1: STEAM

L. Wang-Erlandsson et al.

1 Introduction

Evaporation partitions into biophysical (i.e., transpiration) and physical fluxes (termed here: vegetation interception, floor interception, soil moisture evaporation, and open water evaporation) depending on climate and land-surface properties. In the absence of rain, interception and soil moisture evaporation are ephemeral whereas transpiration continues as long as plants have access to moisture in the root zone. Because of the limited storage capacities of leafs, forest litter, and ground surfaces, high interception rates rely on frequent rainfall (Gerrits et al., 2009). In contrast, transpiration relies more on the rainfall amounts, infiltration rates, and the capacity of the soil in the root zone to retain moisture. The temporal distribution of precipitation affects transpiration only indirectly. Using a conceptual model approach in Zimbabwe, Savenije (2004) estimated relatively high transpiration ratio in wet years, but small in wet months. This is because wet months tend to have high interception that precedes transpiration and consumes the available evaporation energy, whereas wet years tend to receive increased rainfall during the rainy season that stores and transpires into the dry season. High intensity rainfall have also been observed to increase transpiration in a semi-arid forest (Raz-Yaseef et al., 2012), where large storms were more likely to penetrate the top soil and accumulate in the root zone. Another factor that enables transpiration to continue in dry spells and dry seasons is groundwater, which may provide moisture to plants through capillary rise and deep root water uptake (Miguez-Macho and Fan, 2012).

Distinct differences exist in how different land-use types partition evaporation. Mc-Naughton and Jarvis (1983) established in their review that forests generally transpire less and intercept more than short vegetation. Using observation data from flux towers in Europe, Teuling et al. (2010) found that transpiration in grasslands may be higher than in forests when the soil is wet, but declines rapidly with drying soil, whereas trees may continue to transpire long after precipitation has ceased. In general, transpiration ratios reported from field studies in grasslands and croplands are higher (60–90 %) (e.g., Moran et al., 2009; Ferretti et al., 2003; Wang et al., 2012; Wenninger et al.,

ESDD
5, 203–279, 2014

2010) than those from field studies in forests (40–70 %) (e.g., Oishi et al., 2008; Wilson et al., 2001; Calder et al., 1986; Shuttleworth, 1988). However, it should be noted that interception is mostly neglected in grassland and cropland studies, but seldom in forest studies. In addition to differences in vegetation type, characteristics such as tree age may also significantly affect transpiration rates (e.g., Delzon and Loustau, 2005; Fenicia et al., 2009; Forrester et al., 2010).

Most land-surface models and global hydrological models do partition evaporation fluxes, but global partitioning is generally not reported or analysed (e.g., Haddeland et al., 2011; Mueller et al., 2013). The exceptions include evaporative partitioning analyses and improvements made in the Lund–Potsdam–Jena model (LPJ) (Gerten et al., 2005), the Community Land Model (CLM) (Lawrence et al., 2007), and the Joint U.K. Land Environmental Simulator (JULES) (Alton et al., 2009). They report global mean annual transpiration ratios of 65, 41 and 38–48 % respectively. Validation of modelled partitioning is generally qualitative, as most measurements are constrained in space and time. A combination of measurement techniques and satellite observations were recently used to investigate evaporative partitioning at river basin and the global scale (Jasechko et al., 2013), leading to high estimates of the transpiration ratio (80–90 %). However, their results have been challenged by Coenders-Gerrits et al. (2014) who showed that proper accounting of uncertainties reduces transpiration ratio to 35–80 %. The tendency of isotope studies to overestimate transpiration is also acknowledged by Schlesinger and Jasechko (2014) who estimated global transpiration ratio to 61 % based on literature review.

Perhaps as a result of the uncertainties and the scarcity of a global dataset on evaporative partitioning, no research on moisture recycling has considered the separate effects of physical and biophysical evaporation fluxes. The research presented here consists of two separate research papers, which aim to investigate the roles of interception and transpiration in the hydrological cycle. This paper presents and evaluates STEAM (Simple Terrestrial Evaporation to Atmosphere Model), which has been developed to estimate evaporation fluxes based on land use. van der Ent et al. (2014), the

ESDD
5, 203–279, 2014

companion paper, hereafter referred to as Part 2, tracks interception and transpiration fluxes in the atmosphere using the WAM-2layers (Water Accounting Model 2-layers) and analyses the resulting moisture recycling patterns.

The goal of STEAM is to represent different land-use classes with only a limited number of parameters, and yet to produce realistic partitioning between direct and delayed evaporation. This paper further seeks to provide information on the terrestrial residence time scales of evaporation fluxes, and investigate the role of land-use in evaporation partitioning in the model. Diagnosing the role of land-use for evaporative partitioning puts a meaningful physical constraint to model understanding, and allows for a qualitative understanding of when land-use change may influence moisture recycling.

The paper is outlined as follows. Section 2 lists the input data used, and explains data pre-processing performed. Section 3 describes STEAM in detail, including model rationale and structure, parametrisation, and model assumptions. Section 4 explains the experiments and analyses performed using model output. Section 5 presents and discusses model simulation and post-analysis results. The simulated global evaporation is presented by season, partitioning, and land-use, and is evaluated against evaporation, runoff, and irrigation estimates from other studies. In addition, the time scales of evaporative fluxes, and the effect of land-use change are analysed. Finally, Sect. 6 concludes by summarising and discussing our findings, and outlines possible directions for future research.

2 Data

2.1 Meteorological input

Meteorological data were taken from ERA-Interim reanalysis (ERA-I) produced by the European Centre for Medium-Range Weather Forecasts (ECMWF) (Dee et al., 2011). We used evaporation, precipitation, snowfall, snowmelt, temperature at 2 m height, dew point temperature at 2 m height, wind speed in two directions at 10 m height, incoming

ESDD
5, 203–279, 2014

shortwave radiation, and net longwave radiation. All meteorological forcing is given at 3 h and 1.5° latitude × 1.5° longitude resolution. Data used cover latitudes 57° S–79.5° N for the years 1985–2009. The results are presented for the period 1999–2008. The year 2009 is used as spin-up for the moisture recycling backward tracking in WAM-2layers, while data for the years before 1999 are used for the spin-up of STEAM and for simulating evaporation for comparison with the LandFlux-EVAL product (Mueller et al., 2013), (see Sect. 2.3 and Supplement). The period 1999–2008 is chosen for consistency with earlier moisture recycling studies performed in WAM-1layer (van der Ent et al., 2010; van der Ent and Savenije, 2011; Keys et al., 2012).

2.2 Land-surface data

The monthly varying land-surface map used in STEAM consists of 19 land-use types, see Table 1. The first 17 land-use types are based on the Land Cover Type Climate Modeling Grid (CMG) MCD12C1 created from Terra and Aqua Moderate Resolution Imaging Spectroradiometer (MODIS) data (Friedl et al., 2010), and the two irrigated land-use classes are based on the dataset of Monthly Irrigated and Rainfed Crop Areas around the year 2000 (MIRCA2000) V1.1. (Portmann et al., 2010). MODIS data were used for the year 2001 and categorised according to the International Geosphere Biosphere Programme (IGBP) global vegetation classification system. MIRCA2000 is based on the Global Map of Irrigation Areas (GMIA), version 4, but adjusted for overestimation (Siebert and Döll, 2010). The resolution for MODIS is 0.05° and for MIRCA2000 5′. Both datasets were scaled up to 1.5° resolution by maintaining the fractional land-use occupancy, but discarding the spatial position of land-use types within each grid cell.

To create the joint map based on the MODIS and MIRCA2000 data, monthly irrigated land from MIRCA2000 were taken to primarily replace MODIS cropland fraction (13:CRP). If MIRCA2000 exceeds 13:CRP, areas in the cropland/natural mosaic fraction (15:MOS) were taken instead. However, in some grid cells, MIRCA2000 irrigated areas exceeded the sum of both MODIS cropland and cropland/natural mosaic.

ESDD
5, 203–279, 2014

In these cases, we chose to keep the MODIS data and reduce MIRCA 2000 land-use proportionally to its grid cell occupancy. The joint map has a total land area of 133 146 465 km^2 and includes all 19 land-use types and inland waters except big lakes.

Soil texture data has been taken from the Harmonized World Soil Database (HWSD) (FAO/IIASA/ISRIC/ISSCAS/JRC, 2012) and we assigned volumetric soil moisture content at saturation, field capacity and wilting point based on the United States Department of Agriculture (USDA) soil classification (Saxton and Rawls, 2006). Top soil saturation, subsoil field capacity and subsoil wilting point have been assigned to the original 30″ resolution, and scaled up to 1.5° by area weighting.

2.3 Validation and comparison data

For validation of the model, composite and model runoff fields from the Global Runoff Data Centre (GRDC) were used (Fekete et al., 2000). The model runoff fields are the simulations of the GRDC Water Balance Model (GRDC-WBM), whereas the composite runoff fields (GRDC-Comp) are the model runoff corrected by observed inter-station discharge (Fekete et al., 2000). The data are given at 0.5° and represent long term annual average. River basin maps were up-scaled to 1.5° from the 30′ Drainage Direction Map (DDM30) (Döll and Lehner, 2002). In addition, we also used ERA-I runoff fields (Balsamo et al., 2011) in our comparison. It should be noted that the ERA-I runoff fields form a separate dataset that does not directly correspond to ERA-I precipitation minus evaporation.

For comparison of model evaporation with other global estimates, we used the long data series from LandFlux-EVAL evaporation benchmark products (Mueller et al., 2013) for the years 1989–2005. This data product consists of a merged synthesis from 5 satellite or observational, 5 land-surface model simulation, and 4 reanalysis datasets. All data have been interpolated to the ERA-I grid of 1.5° spatial resolution before use.

ESDD
5, 203–279, 2014

3 Simple Terrestrial Evaporation to Atmosphere Model

STEAM (Simple Terrestrial Evaporation to Atmosphere Model) is a process-based model assuming water balance at grid cell level. Because of our need to properly quantify evaporation and its seasonal variations, STEAM includes an irrigation module and calculates dynamic seasonal vegetation parameters based on meteorological conditions. For our current research purposes, we have considered it acceptable to disregard groundwater interaction and lateral flows.

STEAM estimates five evaporative fluxes, and is represented by five stocks, see Fig. 1. The vegetation interception stock S_v represents canopy and vegetation surface (such as leafs, branches and stems) that are the first to be wetted by rainfall ($P - P_{sf}$). The evaporation from this stock is vegetation interception E_v, and the water exceeding the storage capacity $S_{v,\,max}$ is throughfall P_{tf}. In most cases, the latter is intercepted by the ground and litter surface, forming a thin layer of the floor interception stock S_f. The evaporation from this stock is floor interception E_f. The remainder is effective precipitation P_{eff}, which is generated when the storage $S_{f,\,max}$ is exceeded. Water that subsequently reaches the unsaturated root zone stock S_{uz} can be evaporated either as soil moisture evaporation E_{sm}, or be taken up by plant roots and transpire as E_t. In addition to these stocks, we assume that water (01:WAT) and wetlands (12:WET) contain open water, and that vegetation may grow directly in water, in wetlands (12:WET) and rice paddies (19:RIC), see Table 2. These waters are represented by the water stock S_w. Open water is replenished by adding water J_{add} that prevents dry-out in the absence of lateral flow routines. Vegetation covered water also receives P_{tf} from vegetation. Runoff is the sum of excess water Q_{uz} (exceeding $S_{uz,\,max}$) from the unsaturated zone and Q_w from the water stock (exceeding $S_{w,\,max}$). The last and fifth stock S_{snow} does not have a limit, and allows snowfall P_{sf} to accumulate until melting occurs. Snowmelt P_{melt} is allowed only if there is snow in S_{snow} and only up to the given amount of snowmelt given by ERA-I. If the daily mean temperature T_{mean} is above 273 K, P_{melt} goes directly to the floor interception stock, otherwise it does not infiltrate and leaves directly as runoff Q_{uz}.

ESDD

5, 203–279, 2014

In case of irrigation, some water is assumed to be spilled to the vegetation I_v, the floor I_f and the water bodies I_w. The parameterisation of the storage capacities are described in Sect. 3.3.3 and all notations are listed in Appendix A.

3.1 Potential evaporation

Total evaporation, the sum of vegetation interception E_v, floor interception E_f, transpiration E_t, soil moisture evaporation E_{sm}, and open water evaporation E_w, is driven by the daily potential evaporation, and restricted by resistances and water availability. The Penman–Monteith equation (Monteith, 1965) is used to estimate the daily potential evaporation $E_{p,\,day}$ [$\mathrm{m\,d^{-1}}$], which is formulated as follows:

$$E_{p,\,day}(r_a) = \frac{\delta R_{net} + \rho_a C_p D_a / r_a}{\rho_w \lambda (\delta + \gamma)} \tag{1}$$

where δ [$\mathrm{kPa\,K^{-1}}$] is the gradient of the saturated vapour pressure function, R_{net} [$\mathrm{MJ\,m^{-2}\,d^{-1}}$] is the net radiation, C_p [$1.01 \times 10^{-3}\,\mathrm{MJ\,kg^{-1}\,K^{-1}}$] is the specific heat of moist air at constant pressure, D_a [kPa] is the vapour pressure deficit, ρ_a [$\mathrm{kg\,m^{-3}}$] is the density of air, ρ_w [$\mathrm{kg\,m^{-3}}$] is the density of water, λ [$\mathrm{MJ\,kg^{-1}}$] is the latent heat of water vaporisation, γ [$\mathrm{kPa\,K^{-1}}$] is the psychrometric constant, and r_a [$\mathrm{d\,m^{-1}}$] is the aerodynamic resistance. Note that r_a is represented by $r_{a,\,v}$ for vegetation, $r_{a,\,f}$ for floor and $r_{a,\,w}$ for water. As the ground heat flux averaged over a diurnal cycle is often near zero, we neglect this term. The calculations of δ, D_a, λ, γ and the different r_a are given in Appendix B1. The potential evaporation $E_{p,\,day}$ in Eq. (1) does not include surface stomatal resistance $r_{s,\,st}$ for transpiration or surface soil moisture resistance $r_{s,\,sm}$ for soil moisture evaporation. Thus, we introduce k, which is expressed as a function of a surface resistance r_s and an aerodynamic resistance r_a:

$$k(r_s, r_a) = \left(1 + \frac{r_s}{r_a}\frac{\gamma}{\delta + \gamma}\right)^{-1}. \tag{2}$$

ESDD
5, 203–279, 2014

The surface stomatal resistance $r_{s,st}$ is calculated based on the Jarvis–Stewart stress function and optimal temperature based on latitude and altitude, see Appendix B2 for details. The soil moisture resistance $r_{s,sm}$ is applied to soil evaporation and estimated based on the soil moisture content of the top soil layer (Bastiaanssen et al., 2012):

$$r_{s,sm} = r_{s,sm,min} \Theta_{top}^{-3} \tag{3}$$

where $r_{s,sm,min}$ is the minimum surface soil moisture resistance assumed as 3.5×10^{-4} $d\,m^{-1}$, and Θ_{top} [–] is the effective saturation expressed as:

$$\Theta_{top} = \frac{\theta_{top,n} - \theta_{top,res}}{\theta_{top,sat} - \theta_{top,res}}. \tag{4}$$

Since there is no explicit top soil storage in STEAM, top soil moisture at the present time $\theta_{top,n}$ [–] is derived daily based on the inflow to the unsaturated storage and top soil moisture from the previous day $\theta_{top,n-1}$ (Pellarin et al., 2013):

$$\theta_{top,n} = \theta_{top,n-1} e^{-\Delta n/\chi} + (\theta_{sat} - \theta_{top,n-1})(1 - e^{-P_{eff}/y_{top}}) + \theta_{top,res} \tag{5}$$

where Δn is the time step of 24 h, $\theta_{top,res}$ is the volumetric residual soil moisture content assumed as 0.01, y_{top} is the top soil depth, and χ is the dry out parameter which varies with clay content of the top soil. The assumed y_{top} is 0.03 m. In Pellarin et al. (2013), the values used for y_{top} were 0.05 m and 0.1 m, but we considered that a shallower depth is more relevant for estimating soil moisture evaporation stress. The dry out parameter χ is estimated using the following semi-empirical equation:

$$\chi = \frac{y_{top}}{0.1} \max\left[\chi_{min}, 32 \ln\left(\eta_{clay} + 174\right)\right] \tag{6}$$

where η_{clay} is the clay content [%] and χ_{min} is the minimum of χ taken as 60 h.

ESDD
5, 203–279, 2014

3.2 Actual evaporation

Potential evaporation in STEAM is used to evaporate moisture in the following logical sequence: vegetation interception, transpiration, floor interception, and soil moisture evaporation. The diurnal distribution of ERA-I 3 h evaporation is used to scale down the daily potential evaporation $E_{\mathrm{p,\,day}}$ to 3 h time step. Hence:

$$E_{\mathrm{v,\,lu,\,vs}} = E_{\mathrm{v,\,lu,\,vw}} = \min\left(\frac{S_{\mathrm{v,\,lu}}}{\Delta t}, E_{\mathrm{p}}\left(r_{\mathrm{a,\,v}}\right)\right) \tag{7}$$

$$E_{\mathrm{t,\,lu,\,vs}} = \min\left(\frac{S_{\mathrm{uz,\,lu}}}{\Delta t}, \max\left\{0, \left[E_{\mathrm{p}}\left(r_{\mathrm{a,\,v}}\right) - E_{\mathrm{v,\,lu,\,vs}}\right] \cdot k\left(r_{\mathrm{a,\,v}}, r_{\mathrm{s,\,st}}\right)\right\}\right) \tag{8}$$

$$E_{\mathrm{f,\,lu,\,vs}} = \min\left(\frac{S_{\mathrm{f,\,lu}}}{\Delta t}, \max\left[0, E_{\mathrm{p}}\left(r_{\mathrm{a,\,f}}\right) - E_{\mathrm{v,\,lu,\,vs}} - E_{\mathrm{t,\,lu,\,vs}}\right]\right) \tag{9}$$

$$E_{\mathrm{sm,\,lu,\,vs}} = \min\left(\frac{S_{\mathrm{uz,\,lu}}}{\Delta t}, a\right) \tag{10}$$

$$a = \max\left\{0, \left[E_{\mathrm{p}}\left(r_{\mathrm{a,\,f}}\right) - E_{\mathrm{v,\,lu,\,vs}} - E_{\mathrm{t,\,lu,\,vs}} - E_{\mathrm{f,\,lu,\,vs}}\right] \cdot k\left(r_{\mathrm{a,\,f}}, r_{\mathrm{s,\,sm}}\right)\right\},$$

where the first subscript (v, t, f or sm) denotes an individual evaporative flux, the second (lu) the land-use type ID (see Table 1) and the third subscript (vs, vw or ow) denotes the type of vegetation-water occupancy (see Table 2). Thus, for the fraction of vegetation in water ϕ_{vw} in wetlands and rice paddies, there is no floor interception or soil evaporation. Here, transpiration is preceded by vegetation interception just as for the fraction of vegetation in soil ϕ_{vs}, whereas open water evaporation takes the position of floor interception in the evaporation sequence and is preceded by both vegetation

ESDD
5, 203–279, 2014

interception and transpiration:

$$E_{\mathrm{t,\,lu,\,vw}} = \min\left(\frac{S_{\mathrm{w,\,lu}}}{\Delta t}, \max\left\{0, \left[E_{\mathrm{p}}\left(r_{\mathrm{a,\,v}}\right) - E_{\mathrm{v,\,lu,\,vw}}\right] \cdot k\left(r_{\mathrm{a,\,v}}, r_{\mathrm{s,\,st}}\right)\right\}\right) \tag{11}$$

$$E_{\mathrm{w,\,lu,\,vw}} = \min\left(\frac{S_{\mathrm{w,\,lu}}}{\Delta t}, \max\left[0, E_{\mathrm{p}}\left(r_{\mathrm{a,\,w}}\right) - E_{\mathrm{v,\,lu,\,vw}} - E_{\mathrm{t,\,lu,\,vw}}\right]\right). \tag{12}$$

For the water land-use type and the fraction of open water ϕ_{ow} in wetlands, evaporation is expressed as:

$$E_{\mathrm{w,\,lu,\,ow}} = \min\left(\frac{S_{\mathrm{w,\,lu}}}{\Delta t}, \max\left[0, E_{\mathrm{p}}\left(r_{\mathrm{a,\,w}}\right)\right]\right). \tag{13}$$

The total of an evaporation flux from wetland (12:WET) or rice paddy (19:RIC) is determined by the weighted sum based on the fractions of vegetation covered soil ϕ_{vs}, vegetation covered water ϕ_{vw}, and open water ϕ_{ow} (see also Table 2):

$$E_{j,\mathrm{lu}} = \phi_{\mathrm{lu,\,vs}} E_{j,\mathrm{lu,\,vs}} + \phi_{\mathrm{lu,\,vw}} E_{j,\mathrm{lu,\,vw}} + \phi_{\mathrm{lu,\,ow}} E_{\mathrm{w,\,lu,\,ow}} \tag{14}$$

where $E_{j,\mathrm{lu}}$ is an evaporation flux of the land-use type lu.

Subsequently, the total of an evaporation flux from a grid cell is determined by the weighted sum of the land-use types:

$$E_j = \sum_{\mathrm{lu}=1}^{\mathrm{lu}=19} \phi_{\mathrm{lu}} E_{j,\mathrm{lu}} \tag{15}$$

where ϕ_{lu} is the land-use occupancy fraction of the land-use type lu (see Table 2).

3.3 Representation of land use

3.3.1 Primary land-use parameters

The parameters used to describe land-use include maximum and minimum leaf area index $i_{\mathrm{LA,max}}$ and $i_{\mathrm{LA,min}}$, maximum and minimum plant height h_{max} and h_{min}, depth of

ESDD
5, 203–279, 2014

the unsaturated zone (or rather active rooting depth) y_{uz}, albedo α, minimum stomatal resistance $r_{s,st,min}$ and floor roughness $z_{0,f}$. Land-use parameters considered include those used in other large-scale land-surface or hydrological models (Federer et al., 1996; van den Hurk et al., 2000; van den Hurk, 2003; Zhou et al., 2006; Bastiaanssen et al., 2012), and studies of specific land-use properties (Scurlock et al., 2001; Zeng, 2001; Breuer et al., 2003; Kleidon, 2004). The range of parameters in the literature can sometimes be significant and contradictory, due to discrepancies in scale, parameter definitions, and methods of parameter estimation. The choice of land-use parameters is therefore not simply taken as a mean from the literature values investigated, but rather based on the preservation of the internal consistency of STEAM, manual calibration and priority for literature values with higher relevance. The land-use parameters used in the model are shown in Table 3.

3.3.2 Phenology represented by growing season index

The growing season index i_{GS} (Jolly et al., 2005) varies between 0 and 1, and is used to determine the seasonal variations of leaf area i_{LA}. We formulate i_{GS} in STEAM as follows:

$$i_{GS} = f(T_{min})\, f(N)\, f(\theta_{uz}). \tag{16}$$

Note that the last stress function of soil moisture $f(\theta_{uz})$ is a modification of the original expression for i_{GS}, where vapour pressure deficit D_a was used as a proxy for soil moisture (Jolly et al., 2005). However, since soil moisture is calculated in STEAM, it makes sense for us to use the soil moisture stress function to replace the original vapour

ESDD
5, 203–279, 2014
Interception and transpiration – Part 1: STEAM
L. Wang-Erlandsson et al.

pressure stress function. The stress functions are expressed as:

$$f\left(T_{\min}\right)=\begin{cases}0 & T_{\min}\leq T_{\min,\,\mathrm{low}}\\ \frac{T_{\min}-T_{\min,\,\mathrm{low}}}{T_{\min,\mathrm{high}}-T_{\min,\mathrm{low}}} & T_{\min,\mathrm{high}}>T_{\min}>T_{\min,\mathrm{low}},\\ 1 & T_{\min}\geq T_{\min,\mathrm{high}}\end{cases}\tag{17}$$

$$f(N)=\begin{cases}0 & N\leq N_{\mathrm{low}}\\ \frac{N-N_{\mathrm{low}}}{N_{\mathrm{high}}-N_{\mathrm{low}}} & N_{\mathrm{high}}>N>N_{\mathrm{low}},\\ 1 & N\geq N_{\mathrm{high}}\end{cases}\tag{18}$$

$$f\left(\theta_{\mathrm{uz}}\right)=\begin{cases}0 & \theta_{\mathrm{uz}}\leq\theta_{\mathrm{uz,\,wp}}\\ \frac{\left(\theta_{\mathrm{uz}}-\theta_{uz,\mathrm{wp}}\right)\left(\theta_{\mathrm{uz,\,fc}}-\theta_{\mathrm{uz,\,wp}}+c_{\mathrm{uz}}\right)}{\left(\theta_{\mathrm{uz,\,fc}}-\theta_{\mathrm{uz,\,wp}}\right)\left(\theta_{\mathrm{uz}}-\theta_{\mathrm{uz,\,wp}}+c_{\mathrm{uz}}\right)} & \theta_{\mathrm{uz,\,wp}}<\theta_{\mathrm{uz}}<\theta_{\mathrm{uz,\,fc}},\\ 1 & \theta_{\mathrm{uz}}\geq\theta_{\mathrm{uz,\,fc}}\end{cases}\tag{19}$$

where the lower sub-optimal minimum temperature $T_{\min,\,\mathrm{low}}$ is 271.15 K, and the higher $T_{\min,\,\mathrm{high}}$ is 278.15 K. The lower sub-optimal threshold day length N_{low} is assumed to be 36 000 s, and the higher N_{high} is 39 600 s (Jolly et al., 2005). $T_{\min}$ is taken from the coldest 3 h ERA-I temperature of the day. Calculation of day length N is detailed in Appendix B3. c_{uz} is the soil moisture stress parameter fixed at 0.07 (Matsumoto et al., 2008). The soil moisture content θ_{uz} is $S_{\mathrm{uz}}/y_{\mathrm{uz}}$, where S_{uz} [m] is the soil moisture and y_{uz} [m] is the depth of the unsaturated root zone. To prevent unrealistically unstable fluctuations in leaf area, the mean $i_{\mathrm{GS},21}$ of the past 21 days is used to scale i_{LA} between $i_{\mathrm{LA,max}}$ and $i_{\mathrm{LA,min}}$:

$$i_{\mathrm{LA}}=i_{\mathrm{LA,min}}+i_{\mathrm{GS},21}\left(i_{\mathrm{LA,max}}-i_{\mathrm{LA,min}}\right).\tag{20}$$

3.3.3 Storage capacities

The storage capacity determines the maximum water availability for the evaporation flux of concern. We derived vegetation interception storage capacity $S_{\mathrm{v,\,max}}$ [m] from

ESDD
5, 203–279, 2014

the monthly i_{LA} based on the storage capacity factor c_{sc} of roughly 0.2 reported by for example de Jong and Jetten (2007) and used in van den Hoof et al. (2013):

$$S_{v,\max} = c_{sc} c_{AR} i_{LA}, \tag{21}$$

where c_{AR} is the area reduction factor introduced to compensate for rainfall heterogeneity in space and time. The relationship between i_{LA} and vegetation interception storage varies with vegetation type and a strong relationship has not yet been established. In fact, Breuer et al. (2003) even suggests that no general relationship can be established across vegetation types due to the inherent differences in vegetation structures. Nevertheless, vegetation stock linked to i_{LA} has proven to be useful in many cases where there is a lack of detailed vegetation information.

We assume c_{AR} to be 0.4 for STEAM running with a 3 h time step at the 1.5° scale. Area reduction factors have originally been developed to establish a relationship between average precipitation and extreme precipitation of a region, but can be analogously used to reduce interception storage capacity. In an example diagram obtained from catchment analyses (Shuttleworth, 2012), areas larger than 10 000 km^2 have an area reduction factor up to approximately 0.6. In STEAM, grid cell areas with 1.5° resolution are 10 000 km^2 already at 68° N, and grow to almost 28 000 km^2 at equator. Ideally, c_{AR} should vary with the area considered and rainfall duration, but by lack of well-established functions, we consider $c_{AR} = 0.4$ to be acceptable.

The floor interception storage capacity $S_{f,\max}$ [m] is modelled as a function of the leaf area and a certain base value:

$$S_{f,\max} = c_{sc} c_{AR} \left[1 + 0.5\left(i_{LA,\max} + i_{LA,\min}\right)\right]. \tag{22}$$

The floor storage capacity increases in areas with vegetation due to litter formation from fallen leafs, and the base value is considered because wetting of the surface always occur irrespective of the land cover. However, ground litter is assumed to have been removed in croplands (i.e., 13:CRP, 15:MOS, 18:IRR, and 19:RIC). Thus, $S_{f,\max}$

ESDD
5, 203–279, 2014

[m] for crops corresponds to that of bare ground:

$$S_{\mathrm{f,\,max,\,crops}} = c_{\mathrm{sc}} c_{\mathrm{AR}}. \tag{23}$$

As a result of the large grid scale (reflected in the area reduction factor), the interception storages in STEAM are smaller than those normally found in point scale field studies. For example, the vegetation interception storage capacity at the maximum i_{LA} of 5.5 is 0.44 mm, which is about a third of the 1.2 mm reported in a summer temperate forest (Gerrits et al., 2010) and a fraction of the 2.2 to 8.3 mm per unit projected crown in a tropical rainforest site (Herwitz, 1985).

The storage capacity of the unsaturated root zone $S_{\mathrm{uz,\,max}}$ is assumed to be reached at field capacity:

$$S_{\mathrm{uz,\,max}} = \theta_{\mathrm{fc}} y_{\mathrm{uz}}. \tag{24}$$

3.3.4 Irrigation

Irrigation water supplied is assumed to meet the irrigation requirement and is not restricted by water availability. Net irrigation enters the unsaturated zone and is estimated as a function of soil moisture. In rice paddies (19:RIC), irrigation water simply upholds a 10 cm water level. For non-rice crops (18:IRR), irrigation requirement I_{req} is the amount of water needed to reach field capacity in the unsaturated root zone:

$$I_{\mathrm{req}} = \max\left[0, \frac{y_{\mathrm{uz}}\left(\theta_{\mathrm{uz,\,fc}} - \theta_{\mathrm{uz}}\right)}{\Delta t} - \frac{S_{\mathrm{uz,\,lu}}}{\Delta t}\right]. \tag{25}$$

However, because a certain amount of irrigation water applied is always lost due to inefficiencies in the system, an irrigation efficiency should be applied in order to correctly estimate runoff and water withdrawal. In STEAM, we assume the gross irrigation I_{g} to be twice the I_{req}. Although irrigation efficiency in practice varies greatly with irrigation technique, crop type and country (Rohwer et al., 2007), we consider our

ESDD
5, 203–279, 2014

simplification acceptable since the gross irrigation assumption affects evaporation (our major concern) less than for example runoff and water withdrawal. Of gross irrigation applied to irrigated non-rice crops (18:IRR), 15 % is directed to the vegetation interception stock S_{v}, and 85 % to the floor interception stock S_{f}. Of the gross irrigation applied to rice paddies (19:RIC), 5 % is directed to vegetation interception stock S_{v}, 5 % to the floor interception stock S_{f} (assuming inter-paddy pathways), and 90 % to the water stock S_{w}.

4 Analyses of model evaporation output

4.1 Time scales of evaporation fluxes

The time scales τ_{ts} of the evaporation fluxes is defined as the mean stock over the mean flux rate of concern j:

$$\tau_{\mathrm{ts},j} = \frac{\overline{S_j}}{\overline{E_j}}. \tag{26}$$

Figure 1 shows the stock of origin for each evaporation flux. Because both E_{sm} and E_{t} come from S_{uz}, we assumed a stock of soil moisture evaporation $S_{\mathrm{uz,sm}}$ and a stock of transpiration $S_{\mathrm{uz,t}}$. To obtain $S_{\mathrm{uz,sm}}$, we multiplied θ_{top} with the assumed top soil depth y_{top}. To obtain the stock $S_{\mathrm{uz,t}}$, $S_{\mathrm{uz,sm}}$ was subtracted from the total water available in the unsaturated zone S_{uz}:

$$S_{\mathrm{uz,t}} = S_{\mathrm{uz}} - S_{\mathrm{uz,sm}} = \theta_{\mathrm{uz}} y_{\mathrm{uz}} - \theta_{\mathrm{top}} y_{\mathrm{top}}. \tag{27}$$

Because the time scale becomes infinite when the flux approaches zero, time scales are not given for areas where the mean evaporation flux is below 0.01 mm d^{-1}. Coastal areas where the land area fraction is less than 100 % are removed from the time scale analysis. The time scale for open water evaporation is not calculated.

ESDD
5, 203–279, 2014

4.2 Validation by runoff comparison

Comparisons have been made between runoff from the GRDC composite dataset (which is observation-corrected runoff simulation data), the GRDC water balance model, and ERA-I runoff, see Sect. 2.3. Standard deviation is calculated based on the difference between the mean river basin runoff of each dataset and the GRDC composite dataset. Although global runoff data still involve large uncertainties, particularly in parts of Africa, it can still be useful as an independent source of information to validate global evaporation estimates.

Runoff fields from STEAM have been derived from subtracting mean evaporation and mean snow storage changes from mean precipitation over the years 1999–2008. Snow storage changes were subtracted because snow accumulated in glaciers may carry over storage from year to year. Otherwise, most storage changes may be neglected at an annual time scale.

4.3 Sensitivity to precipitation

We checked the sensitivity of STEAM evaporation to precipitation by applying a 5 % uniform reduction of precipitation. This check is performed because STEAM is forced by ERA-I precipitation reanalyses data, which is considered to be on the high side. For the 1999–2008, the mean global ERA-I precipitation is 118 236 $km^3 year^{-1}$ for a land area of 133 146 465 km^2. Other reported terrestrial precipitation values include 111 000 $km^3 year^{-1}$ (Oki and Kanae, 2006), 109 500 $km^3 year^{-1}$ from CRU, 111 200 $km^3 year^{-1}$ from PREC/L, and 112 600 $km^3 year^{-1}$ from GPCP (Trenberth et al., 2007).

ESDD
5, 203–279, 2014

5 Results and discussion

5.1 Evaporation estimation

STEAM estimates global annual terrestrial evaporation as 555 mm year^{-1} (i.e., 73 835 km^3 year^{-1}) for a land area of 133 146 465 km^2 and for the period 1999–2008. This is comparable to current global evaporation datasets. In the Water Model Intercomparison Project (WaterMIP), the range of evaporation given by eleven models was 415–585 mm year^{-1} for the period 1985–1999 forced with WATCH meteorological data (Haddeland et al., 2011). By subtracting global runoff from precipitation products for the years 1984–2007, Vinukollu et al. (2011) arrived at global evaporation rates of 488–558 mm year^{-1} (i.e., 64 000–73 000 km^3 year^{-1}). In the LandFlux-EVAL multi-data set synthesis, the global mean evaporation was 493 mm year^{-1} as given by a combination of land-surface model simulations, observational dataset, and reanalysis data for both the period of 1989–1995 and 1989–2005 (Mueller et al., 2013). In the LandFlux comparison, evaporation from the participating land-surface models is lower than those from the reanalyses products. Overall, STEAM evaporation estimate is well in between these two types of products, see Supplementary materials.

In STEAM, the dominating evaporation flux is transpiration E_t (59 %), followed by vegetation interception E_v (21 %), floor interception E_f (10 %), soil moisture evaporation E_{sm} (6 %) and lastly, open water evaporation E_w (4 %). The global distribution of the annual mean evaporation fluxes is shown in Figs. 2 and 3 (as percentage of total evaporation). January and July evaporation are shown in Appendix C. It is shown that transpiration dominates in the densely vegetated areas in the tropics. In addition, transpiration rates increase over the boreal forests during the Northern Hemisphere summer. Land-use specific evaporation partitioning is presented and discussed in Sect. 5.3.1.

Table 4 provides an overview of evaporative partitioning values in the literature and in STEAM. First, we note that STEAM transpiration ratio is in good agreement with the literature compilation results presented by Schlesinger and Jasechko (2014) and the LPJ estimate by Gerten et al. (2005), but higher than other land-surface model simulations

(Alton et al., 2009; Lawrence et al., 2007; Choudhury et al., 1998; Dirmeyer et al., 2006). An exceptionally high global transpiration ratio of 80–90 % was estimated by Jasechko et al. (2013) using an isotope and water balance method, but criticism shows that this is an unreliable and unlikely high estimate (Coenders-Gerrits et al., 2014). Second, the order of dominant flux ($E_t > E_v > (E_f + E_{sm})$) in STEAM is in agreement with the satellite based study of Miralles et al. (2010), but the three modelling studies with reported interception values (Lawrence et al., 2007; Choudhury et al., 1998; Dirmeyer et al., 2006) all report higher soil evaporation than vegetation interception.

Some discrepancies between studies will always be explained by inherent differences in represented areas of terrestrial regions, inland waters, and land-use types. For example, while STEAM includes IGBP and MIRCA2000 land-use types, JULES uses plant functional types (Alton et al., 2009). Aside from differences in data input and parametrisation, the differences in model processes could play a role in explaining the differences in partitioning. For example, we note that STEAM includes irrigation, which has been left out in some of the land-surface model simulations we are comparing here (Lawrence et al., 2007; Alton et al., 2009). In addition, STEAM does not assume any fractions of bare soil within a land-use type, but employs a sequential evaporation process (E_v and E_t precede E_f and E_{sm}) that implicitly takes bare soil into account (i.e., regions with large bare soil areas are likely to have lower i_{LA} and allow more evaporation from floor and soil moisture). As Fig. 2 shows, E_{sm} is clearly suppressed in the tropical and most densely vegetated areas, and less so in the subtropics and sparsely vegetated areas. Furthermore, increasing the area reduction factor (Eq. 22) for floor interception storage capacity (because floor remain wet longer that vegetation, see Sect. 5.2) could rightly increase the floor interception, but also introduce yet another uncertain assumption. Nevertheless, STEAM results lie well within the reported range.

5.2 Terrestrial time scale of evaporation fluxes

There is a striking difference in time scales between the interception and transpiration. The modelled global average time scale (Eq. 26) is 1.4 h for E_v and 8.2 h for E_f, but

41 days for E_{sm} and 275 days for E_t in areas with mean evaporation rate higher than 0.01 mm d^{-1}. The evaporation from vegetation cover and floor is large compared to their respective stocks, resulting in small temporal scales for interception. In contrast, the stocks in the unsaturated zone are many times larger than the interception stocks, and cause the time scales of soil moisture evaporation and transpiration to extend to days and months. Note, however, that the spatial and temporal variations are large.

Figure 4 shows the spatial distribution of mean terrestrial residence time scales (i.e., stock divided by flux) of the partitioned evaporation fluxes (Eq. 26). We see that time scales are in general prolonged over the tropics, and over the cold northern latitudes. Over the tropics, evaporation rates are high, but the stocks are also relatively larger. In addition, as vegetation interception and transpiration are relatively high in the dense tropics, floor and soil moisture evaporation are suppressed and their time spent on the land is prolonged.

The temporal variation of the evaporation fluxes in the Northern and the Southern Hemispheres is displayed in Fig. 5. Seasonality is distinct for all evaporation fluxes, except for vegetation interception because of limited interference with plant physiology that allows it to continue into the winter season (see Appendix C). While the mean hemisphere transpiration time scale can extend to over 300 days in the Northern Hemisphere winter, it falls below 100 days in the summer. We note that interception is likely to occur within the rainy period, whereas transpiration may have a substantial time lag between the moment water enters the soil and exit through a plant's stomata. This also explains why transpiration dominates in the dry season. In Part 2, the effect of the terrestrial moisture recycling and atmospheric residence times will be analysed.

5.3 Land-use specific analyses

5.3.1 Evaporation contribution by land use

Evaporation contribution per land-use type are listed in Table 5, and compared to the other studies in Table 6. The highest evaporation rates are found in irrigated land, evergreen broadleaf forests, and open water. This is followed by wetlands, savannah, deciduous broadleaf forest, natural mosaic, woody savannah, mixed forest, and rainfed croplands. Evaporation rates in the lower tier include contribution from needleleaf forests, grassland, and shrubland. In general, STEAM evaporation is comparable to the estimates of Gordon et al. (2005), the compilation results of Schlesinger and Jasechko (2014) (based on Mu et al., 2011), and the field data from Rockström et al. (1999). The mixed forest evaporation estimate in STEAM is double that of Gordon et al. (2005), but the area is also very different, suggesting substantial differences in definition. Closed shrubland in STEAM also produces higher evaporation rates, but because the numbers are for shrublands in general and not closed shrubland in particular, the shrubland comparison is inevitably inconclusive. Some caution is warranted in comparing evaporation rates across studies. Nevertheless, this comparison shows that evaporation estimates in STEAM are within the range of previous estimates.

Table 5 also shows the annual average evaporation fluxes as a percentage of total evaporation per land-use class. Transpiration is the dominant evaporation flux in almost all land-use types: 50–64 % in forests, 61 % in grassland, 72 % in cropland, and 58–65 % in shrublands. The exceptions are barren land (17:BAR) where soil moisture evaporation is higher, and for snow and water, which do not transpire, because of a lack of vegetation. Among the more vegetated land-use types, vegetation interception ratios are highest in forests (21–37 % of E), followed by cropland (17 %), and lowest in the sparsely vegetated land-use types: shrubland, savannah, grassland, wetland, and urban land (10–14 %). Floor interception values follow the pattern of vegetation interception. Thus, floor interception is generally higher than soil moisture evaporation in forests, whereas soil moisture evaporation equals or exceeds floor interception more often in shrublands and crops.

Reported land-use specific evaporative partitioning in previous research is scarce at the global scale. Lawrence et al. (2007) do not report CLM3-simulated evaporative partitioning by land use, but map figures indicate that their soil evaporation are higher and canopy interception are lower in savannah, grassland, and shrubland occupied areas

ESDD
5, 203–279, 2014

compared to STEAM. Transpiration ratios are comparable with STEAM in forested and savannah areas, but are much lower (down to < 30 %) in the western US, India, south-eastern China, and South Africa. Alton et al. (2009) report global mean transpiration ratios of 49–65 % in forests, 32–60 % in grassland, and 44–51 % in shrublands. The order of magnitude is similar to STEAM, but transpiration ratios for shrublands are lower. Schlesinger and Jasechko (2014) compiled satellite-based estimates from Mu et al. (2011) and arrived at 70 % transpiration in tropical forests, 55–67 % in other forests, and 57–62 % in grasslands. Choudhury et al. (1998) used a biophysical process-based model, and estimated transpiration ratio to amount to 56–77 % in three rainforest regions, 63–82 % in three savannah regions, and 37–82 % in seven cropland areas. Transpiration for river basins shown in the isotope study of Jasechko et al. (2013) show transpiration ratios above 70 % in grassland dominated areas in western U.S van den Hoof et al. (2013) evaluated model performance against sites in temperate Europe, and reported transpiration rates of 47–78 % at eight forest sites, and 59–79 % at three grassland sites. Overall, STEAM falls well in the range of the reported evaporation partitioning ratios.

STEAM estimates vegetation interception ratio as 18 % of rainfall in evergreen broadleaf forest, 17 % in deciduous broadleaf forest, and 18–20 % in needleleaf forest. In comparison, Miralles et al. (2010) arrived at higher canopy interception in coniferous (22 %) and deciduous forest (19 %) than in tropical forest (13 %) using satellite data analysis and literature review. Thus, interception ratios are comparable, except for tropical forest. In an interception scheme comparison study, Wang et al. (2007) found that the scheme that took rainfall type into account also performed the best, (i.e., closest to interception ratios reported in a selection of field studies). Although STEAM uses an area reduction factor to scale interception, this may simply not be enough in the tropical, convective rainfall regimes. On the other hand, Miralles et al. (2010) may also have underestimated the interception ratios in the tropics. First, their model clearly underestimates interception ratios in areas where validation field studies in the tropics report high values. Of the six tropical field studies reporting interception ratios > 15 %,

ESDD
5, 203–279, 2014

their model only correctly estimated one of them, and underestimated the rest. Second, the selection of field study values they used for validation might be biased towards low interception values. The highest interception ratio among their selection was 13.5 % in the Amazon. However, studies have shown higher interception ratios than that. For example, Cuartas et al. (2007) reported 16.5 % for two years in Central Amazon, Franken et al. (1992) reported 19.8 % in Central Amazon, and Tobón Marin et al. (2000) reported 12–17 % in Colombian Amazon over four years. Interestingly, Cuartas et al. (2007) also showed that the differences in dry and normal years can differ substantially: 13.3 % in a normal year and 22.6 % in a dry year. Thus, we consider our results realistic.

5.3.2 Irrigation

The simulated mean gross irrigation is 1969 $km^3 year^{-1}$ for the considered years 1999–2008, and the simulated mean increase in evaporation from irrigation for the years 1999–2008 is 1155 $km^3 year^{-1}$. The irrigation hotspots in especially India, south-eastern China, and the central US coincide well with where evaporation is enhanced by irrigation input. Our estimates are comparable to previous estimates. Gross irrigation was estimated at 2500 $km^3 year^{-1}$ by Döll and Lehner (2002), at 2353 $km^3 year^{-1}$ by Seckler et al. (1998), and at 1660 $km^3 year^{-1}$ by Rost et al. (2008). The latter study did, however, not take into account recharge to the groundwater. Evaporation contribution by irrigation was simulated at 1100 $km^3 year^{-1}$ by Döll and Lehner (2002). While higher evaporation contributions have also been reported in the literature, such as 2600 $km^3 year^{-1}$ by Gordon et al. (2005), they could possibly be explained by differences in methods and irrigation maps. Gordon et al. (2005) does for example not take into account variations in growing area over the year, or separate rice from other types of crops. Given the uncertainties, the modeling results are considered acceptable in terms of total amounts.

ESDD
5, 203–279, 2014

5.3.3 Land-use change experiment

As an experiment, we swapped the land-use parametrisation for selected land-use types while forcing the model with the same meteorological data. The aim of the experiment was to investigate the role of land-use parametrisation for the simulation of evaporation fluxes. The results of the experiment are shown in Fig. 6. It is shown that the parametrisation of barren land (17:BAR) decreases total evaporation, whereas irrigation (18:IRR) consequently leads to evaporation increase. Only floor interception is increased slightly in the evergreen broadleaf forest (03:EBF) location, probably because the evaporation fluxes that precede floor interception are much lower for barren land. It is also worth noting that the relative changes in total evaporation and transpiration are generally smaller than for other fluxes. Notably, replacing evergreen broadleaf forest or mixed forests with shrubland, savannah, or grassland seems to dramatically decrease vegetation interception, without changing total evaporation. Likewise, applying forest parametrisation to shrubland, savannah or grassland regions may more than double vegetation interception, but without changing total evaporation due to a decrease in soil moisture evaporation and transpiration.

Using the barren land parametrisation (17:BAR) in the evergreen broadleaf forest regions (03:EBF) decreases the annual total evaporation the most in terms of absolute value ($-457\,\mathrm{mm\,year^{-1}}$). Despite the lack of explicit meteorological feedback, simulated absolute decrease in STEAM is comparable with previous simulations using general circulation models and the soil-vegetation-boundary layer model PEGASUS (Bagley et al., 2011), as shown in Table 7. The considered areas and degree of vegetation removal differ between these studies, but the magnitude of change is similar. The evaporation decrease is a result of the combined effects of all changes in land-use parametrisation, including reduced net radiation by increased albedo, reduced water uptake in dry periods by decreased rooting depth, and increased vegetation interception capacity as well as reduced resistance to transpire following decreased leaf area

ESDD
5, 203–279, 2014

index. However, in terms of relative change, the barren land parametrisation causes the most significant evaporation drop in cropland (53 %) and mixed forest (–62 %) areas.

Figure 7 shows the temporal variations of evaporation fluxes in four selected evergreen broadleaf forest regions under different land-use parametrisations. Several observations can be made. First, the irrigated parametrisation (Fig. 7, last column) shows an approximation of evaporation under unrestricted water availability as crop periods are not included. This shows clearly that the dip in evaporation in the Amazon-2 region (southeast Amazonia) is a response to limited water availability. Second, for a given potential evaporation, the different evaporative fluxes tend to compensate for each other when land use is exchanged, adjusting the partitioning, but keeping the total evaporation approximately constant. Conversion to barren land is an exception, as the extremely scarce vegetation considerably restrict the ways to compensate. Third, Fig. 7 shows that transpiration allows evaporation to persist into the dry season in comparison with interception and soil moisture evaporation. In the Amazon-2 region, the total evaporation and transpiration start to dip in June in the EBF parametrisation, but floor interception (see EBF parametrisation) and soil moisture evaporation (see BAR parametrisation) start to drop already in April – a difference of two months.

We note further that evaporation dips considerably in the Amazon-2 region during the dry season when applying the original EBF parametrisation (Fig. 7, first column), but remains high when savannah parametrisation is used (Fig. 7, second column). We acknowledge that this could be an artefact in the model, likely caused by the difference in rooting depth between the SAV (3.5 m) and the EBF (2 m) parametrisation. Although a forest rooting depth of 2 m is employed across many land-surface models, deeper rooting depth have been suggested to lie closer to observations and reduce the dry season sensitivity of forests (Kleidon and Heimann, 2000). Moreover, rooting depth is here modelled as a function of land use and indirectly of soil texture. However, many factor govern root water uptake beside vegetation type, including topography (Gao et al., 2013), soil properties, hydraulic redistribution of soil water by roots (Lee et al., 2005), groundwater table (Miguez-Macho and Fan, 2012), and climate (Feddes et al., 2001). Indeed, root water uptake is a complex process that will require more attention in future model improvements for more realistic land-use change simulation.

These simulated effects are merely the result of land-use change with meteorological forcing remaining equal. Thus, the resulting adjustments in evaporative fluxes are mainly due to changes in i_{GS} and surface (stomatal and soil moisture) and aerodynamic (vegetation and floor) resistances. In reality, these changes in land-use type may not be realised due to biophysical constraints (e.g., evergreen broadleaf forest is not likely to develop in barren land regions). Online coupled simulations with atmospheric models could also include meteorological (precipitation and air humidity) feedbacks that come closer to reality. Nevertheless, this experiment illustrates that changes in partitioning can be significant due to land-use change, even if the change in total evaporation is insignificant.

5.4 Runoff comparison

We estimate the mean annual global runoff (taken as $\overline{P} - \overline{E} - (\overline{\mathrm{d}S_{snow}/\mathrm{d}t})$) at 43 314 km^3 year^{-1} (325 mm year^{-1}, 37 % of $\overline{P}$) for a terrestrial area of 133 146 465 km^2 (including Greenland, excluding Antarctica). Based on discharge data and simulated stream flow simulations, Dai and Trenberth (2002) estimated runoff to be 37 288 ± 662 km^3 year^{-1} (35 % of $\overline{P}$, excl. Greenland and Antarctica). Syed et al. (2010) arrived at 36 055 km^3 year^{-1} based on the global ocean mass balance, Oki and Kanae (2006) reported 45 500 km^3 year^{-1} including groundwater runoff, and the GRDC composite runoff (GRDC-Comp) is about 38 000 km^3 year^{-1} (Fekete et al., 2000). Thus, the STEAM runoff estimate appears to be slightly higher than some of the previous estimates, but lies within the uncertainty range. Differences can partly be explained by the terrestrial area considered in the studies, as well as relatively high P applied (see Appendix D).

STEAM runoff was also compared to GRDC-Comp, GRDC-WBM, and ERA-I runoff data in 13 major river basins of the world, see Figs. 8 and 9a. We included two

ESDD
5, 203–279, 2014

additional STEAM scenarios: one simulation without irrigation, and one with 5 % uniform reduction in precipitation forcing. The largest deviations for both STEAM and ERA-I from the GRDC-Comp runoff are found in the Congo and Nile river basins. However, because Congo precipitation and runoff are particularly uncertain (Tshimanga, 2012), it is hard to say whether our evaporation estimate is correct. As for the Nile river basin, STEAM uses a static land-use map that does not include seasonal variations in wetland size or presence of reservoirs. Since the Nile contains the Sudd, one of the largest wetlands in the world with a highly variable size, evaporation simulation is challenging in this region, even in fine resolution models including complex processes (Mohamed, 2005; Mohamed et al., 2007). In several of the northern river basins (e.g., the Mississippi, Mackenzie, and Danube), STEAM runoff is low in comparison to GRDC-Comp. There could be multiple reasons for this underestimation: our simplified snow simulation, our uniform parametrisation of land-use classes across climate zones or simply uncertainties in the forcing data. In support of the latter, the largest uncertainties in evaporation inferred from precipitation and runoff data occur mainly in the higher latitudes (Vinukollu et al., 2011).

Table 8 shows that the STEAM evaporation is close to the mean evaporation provided by the WaterMIP (Water Model Intercomparison Project) (Haddeland et al., 2011; Harding et al., 2011), while both the simulated runoff and the used precipitation forcing is substantially lower. In contrast, in the Lena river basin, STEAM runoff is in range while both evaporation and precipitation have a high bias. In the Amazon basin, the default STEAM simulation slightly overestimates runoff, but reducing precipitation forcing by 5 % (see the 95 %-*P* run in Fig. 8) brings runoff down to the level in GRDC-Comp. Also the comparison with WaterMIP indicates that high bias in Amazon precipitation translates into high runoff. This effect of precipitation reduction can also be noted in particularly the Brahmaputra–Ganges, Congo, and Nile river basins. This is not surprising, because runoff has been shown to be especially sensitive to precipitation uncertainties when evaporation is not limited by water availability (e.g., Fekete et al., 2004). The

ESDD
5, 203–279, 2014

relative sensitivity of runoff and evaporation fluxes to precipitation is further accounted for in Appendix D.

The standard deviation between the multiyear mean runoffs in GRDC-Comp (which we here consider as the benchmark runoff) and the other runoffs (GRDC-WBM, ERA-I, and STEAM) are shown in Fig. 9b and c. Among the compared datasets, STEAM runoff deviates the most from GRDC-Comp when Congo is included and the least when Congo is excluded. Note also that omitting irrigation in STEAM increases the runoff deviation to GRDC-Comp, and that reducing precipitation decreases this deviation. Thus, the wet bias in ERA-I precipitation probably explains some of the runoff overestimations we have noticed in STEAM.

6 Summary and conclusions

This paper described and evaluated the new global hydrological land-surface model STEAM, which is here used to investigate the properties of different physical and biophysical evaporation fluxes in the hydrological cycle. The essence of STEAM is to produce realistic estimates of terrestrial evaporation based on land use while preserving a simple model structure and parametrisation. Thus, STEAM represents climate-driven phenology, irrigation, and rainfall partitioning, but neglects processes we consider less important for evaporation, such as groundwater flow and lateral flow. We have evaluated STEAM against other modelling studies, global datasets, and field studies. We also showed the terrestrial residence time scales, which are unique images of the spatial and temporal variation for each evaporative flux.

STEAM's total terrestrial evaporation rate is comparable with previous estimates – lower than reanalysis products, but higher than other land-surface models. Reasons for this include that we do not add water in data assimilation as in reanalysis, and compared to other land-surface models we use a relatively high precipitation input and also include irrigation and wetlands. Overall, STEAM simulates global evaporation partitioning realistically. Vegetation interception ratios in forests are comparable with both

ESDD
5, 203–279, 2014

the findings from a global satellite based estimate of interception (Miralles et al., 2010) and with reported values from field studies in the tropics. The global mean transpiration ratio in STEAM is within the uncertainty range: similar to or somewhat higher than other land-surface models, and in line with the recent literature compilation study of Schlesinger and Jasechko (2014). In agreement with previous studies (McNaughton and Jarvis, 1983; de Bruin and Jacobs, 1989; Teuling et al., 2010), STEAM also simulates higher transpiration ratios in short vegetation types than in forests.

Results from a land-use change experiment indicate that STEAM can be used to simulate land-use change effects on terrestrial evaporation. Despite STEAM's simple model structure and the offline simulation set-up, deforestation effects on evaporation are comparable with previous coupled land–atmosphere simulations. In future work, the parameter sensitivity in different meteorological conditions should be tested to better understand how each parameter tunes the model. It would be useful to investigate the evaporation response of different land-use types to a number of perturbations, both for validation and investigation purposes. Crop simulations are at present simplified as their development follow meteorological forcing through the growing season index, rather than sowing and harvesting dates. Vegetation should also preferably be simulated with threshold effects in response to unfavourable meteorological conditions.

In comparison to mean GRDC composite runoff in 13 large river basins, STEAM performs better than both ERA-I and the GRDC Water Balance Model if the Congo (with poor gauging and large runoff uncertainties) is taken out. In a precipitation sensitivity check, we showed that precipitation uncertainty translates into much larger changes in runoff than in evaporation. In the northern river basins, STEAM runoff tends to be lower than the GRDC composite runoff. Explanations could perhaps be sought in the simplified simulations of snow and ice, the climate zone independent land-use parametrisation, uncertainties in forcing data, or in improvements in model structure to better suit the conditions of the northern regions. In the present simulation, the evaporation ratios are generally low in the north and matter less for moisture recycling, but there is room here for future model development.

ESDD
5, 203–279, 2014

The analyses here showed that interception and transpiration are two distinctly different fluxes with different time scales, which vary greatly over the seasons. Because of the differences in time scale, spatial scale (area reduction factor) and timing, the response of different types of evaporation to climate and land-use change is different and still poorly understood. In the agricultural sector, improved partitioning also improves the assessment of the potential to increase crop yields through "vapour shift" from unproductive evaporation fluxes to productive transpiration (Rost et al., 2009). In understanding how the changing climate affects hydrological fluxes (Kleidon and Renner, 2013), correct consideration of the different evaporation mechanisms is useful, because the result of their interaction is different from any single mechanism operating alone. Considerable research efforts have in recent years been directed towards comparing evaporation data from different datasets (e.g., Mueller and Seneviratne, 2011; Haddeland et al., 2011; Jiménez et al., 2011; Trambauer et al., 2014), but it remains a challenge to understand the underlying reasons to those differences. Taking partitioning into account in these analyses may reveal where model assumptions make a difference in evaporation delay time. Further research is needed to narrow down the uncertainties in both evaporation and in partitioning.

The importance of land use for the hydrological cycle, the climate, and the Earth system as a whole has been stressed in many studies (e.g., Feddema et al., 2005; Gordon et al., 2005; Rockström et al., 2009). Thus, if the relative variations in evaporative partitioning are larger than absolute evaporation values following land-use change, closer examination may have implications and provide answers for landscape resilience, drought development, and effects on remote fresh water resources. The latter constitutes the case for investigation in Part 2, the companion paper, for the present day situation. Future research should also extend to land-use change scenario analysis to quantify and improve the assessment of land-use change effects on global fresh water resources.

ESDD
5, 203–279, 2014

Appendix A

Notations

Symbols used in this paper are listed and defined in Table A1.

Appendix B

Model equations

B1 Input variables to the Penman–Monteith equation

The vapour pressure deficit D_a is defined as:

$$D_a = e_s - e_a(T_{dew}), \tag{B1}$$

where e_s [kPa] is the saturated vapour pressure at temperature T_{mean} [K] and estimated from the average of the saturated vapour pressures of the daily maximum and minimum temperature, e_a [kPa] is the vapour pressure of air at height z_{ref} [m], and T_{dew} [K] is the daily mean dew point temperature. Vapor pressure e_a is estimated from the formula below:

$$e_a(T_{dew}) = \frac{0.6108 e_a^{17.27(T_{dew}-273.15)}}{T_{dew} - 35.85}. \tag{B2}$$

For the estimation of e_s, T_{dew} was replaced by T_{max} or T_{min}. The latent heat of water vaporisation λ [MJ kg^{-1}] is expressed as:

$$\lambda = 2.501 - 0.002361(T_{mean} - 273.15). \tag{B3}$$

ESDD
5, 203–279, 2014

Interception and transpiration – Part 1: STEAM

L. Wang-Erlandsson et al.

The gradient δ [kPa K^{-1}] of the saturated vapour pressure function is given by

$$\delta = \frac{4098 \times e_s}{237.3 + (T_{mean} - 273.15)^2}. \quad \text{(B4)}$$

The psychrometric constant γ [kPa K^{-1}] is

$$\gamma = \frac{C_p p}{\xi_{mw} \lambda}, \quad \text{(B5)}$$

where p is the atmospheric pressure [kPa], and ξ_{mw} is the ratio of the molecular weight of water vapour to that for dry air [0.622].

Net radiation is calculated by:

$$R_{net} = (1 - \alpha) R_{sw} - R_{net,\,lw} \quad \text{(B6)}$$

where α is albedo, R_{sw} is the incoming shortwave radiation and $R_{net,\,lw}$ is the outgoing net longwave radiation. In reality, albedo varies with angle of reflection and the surface properties such as snow cover change and ground wetness. Here, we assume α to be fixed for each land-use type, see Table 3.

There are three types of aerodynamic resistances used in STEAM: the aerodynamic vegetation resistance $r_{a,\,v}$, the aerodynamic floor resistance $r_{a,\,f}$, and the aerodynamic water resistance $r_{a,\,w}$. They are expressed as follows (Shuttleworth, 2012):

$$r_{a,\,v} = \frac{\ln \frac{z_{ref} - d}{z_0} \ln \frac{z_{ref} - d}{0.1 z_0}}{u_{ref,\,v} \kappa^2}, \quad \text{(B7)}$$

$$r_{a,\,f} = \frac{\ln \frac{z_{ref,\,f}}{z_{0,f}} \ln \frac{z_{ref,\,f}}{0.1 z_{0,f}}}{u_{ref,\,f} \kappa^2}, \quad \text{(B8)}$$

$$r_{a,\,w} = \frac{4.72 \ln^2 \frac{z_{ref,\,w}}{z_{0,f}}}{1 + 0.536 u_{ref,\,w}}, \quad \text{(B9)}$$

ESDD
5, 203–279, 2014
Interception and transpiration – Part 1: STEAM
L. Wang-Erlandsson et al.

where z_{ref} is the reference height [m], z_0 is the aerodynamic roughness length [m], d is the zero-plane displacement height [m] and u_{ref} is the wind speed [m d^{-1}] at z_{ref}. Wind speed u_{ref} is estimated from wind speed u_{10} given by ERA-I at 10 m z_{10} [m] under the assumption of a logarithmic wind profile and stable neutral atmospheric conditions:

$$u_{ref,f} = u_{10}\frac{\ln\frac{z_{ref,f}}{z_{0,f}}}{\ln\frac{z_{10}}{z_{0,f}}}, \tag{B10}$$

$$u_{ref,w} = u_{10}\frac{\ln\frac{z_{ref,w}}{z_{0,f}}}{\ln\frac{z_{10}}{z_{0,f}}}, \tag{B11}$$

where the reference height $z_{ref,f}$ and $z_{ref,w}$ are 2 m and $z_{ref,v}$ is $2 + h$ [m], with h being the plant height [m]. However, because some vegetation is higher than 10 m, wind speed at 200 m is substituted into the formula to derive wind speeds at lower elevations:

$$u_{ref,v} = u_{10}\frac{\ln\left(\frac{z_{200}}{z_0}\right)}{\ln\left(\frac{z_{10}}{z_0}\right)}\frac{\ln\left(\frac{z_{ref,v}-d}{z_0}\right)}{\ln\left(\frac{z_{200}-d}{z_0}\right)}. \tag{B12}$$

The aerodynamic roughness length z_0 [m] is estimated from:

$$z_0 = \begin{cases} z_{0,f} + 0.29h\sqrt{0.2i_{LA}} & i_{LA} \le 1 \\ 0.3h\left(1-d/h\right) & i_{LA} > 1 \end{cases}. \tag{B13}$$

Zero plane displacement d is estimated from h [m] and i_{LA} [m^2 m^{-2}]

$$d = 1.1h\ln\left[1 + (0.2i_{LA})^{0.25}\right], \tag{B14}$$

$$h = h_{min} + (h_{max} - h_{min})\, i_{LA}/i_{LA,max}. \tag{B15}$$

ESDD
5, 203–279, 2014

B2 Surface stomatal resistance

Surface resistance applies only to transpiration and soil moisture evaporation, since interception and open water evaporation occur without resistance. The surface stomatal resistance $r_{\text{s, st}}$ of vegetation is simulated by the Jarvis–Stewart equation (Stewart, 1988), taking into account of solar radiation, vapour pressure deficit, optimum temperature, and soil moisture stress:

$$r_{\text{s, st}} = \frac{r_{\text{s, st, min}}}{i_{\text{LA,eff}} f\left(R_{\text{sw}}\right) f\left(D_{\text{a}}\right) f\left(T_{\text{mean}}\right) f\left(\theta_{\text{uz}}\right)}, \tag{B16}$$

where $r_{\text{s, st, min}}$ is the minimum surface stomatal resistance dependent on land-use type and specified in the land-use look-up table, $i_{\text{LA,eff}}$ is the effective leaf area index (unit leaf area per unit ground area that is actively participating in transpiration) and f are the four stress functions for incoming showrtwave radiation R_{sw} in W m^{-2}, vapour pressure deficit D_{a}, mean daily temperature T_{mean} and soil moisture θ_{uz} (Stewart, 1988). Effective leaf area index $i_{\text{LA,eff}}$ is adapted from Allen et al. (2006); Zhou et al. (2006) as:

$$i_{\text{LA,eff}} = \frac{i_{\text{LA}}}{0.2 i_{\text{LA}} + 1}. \tag{B17}$$

The stress functions vary between 0 and 1. $f(\theta_{\text{uz}})$ is formulated the same as in Eq. (19) and the others as follows (Jarvis, 1976; Zhou et al., 2006; Matsumoto et al., 2008):

$$f\left(R_{\mathrm{sw}}\right)=R_{\mathrm{sw}}\left(1+c_{\mathrm{R}}/1000\right)\left(c_{\mathrm{R}}+R_{\mathrm{sw}}\right)^{-1}, \tag{B18}$$

$$f\left(D_{\mathrm{a}}\right)=\left[1+\left(D_{\mathrm{a}}/D_{0.5}\right)^{c_{\mathrm{D1}}}\right]^{-1}\left(1-c_{\mathrm{D2}}\right)+c_{\mathrm{D2}}, \tag{B19}$$

$$f\left(T_{\mathrm{mean}}\right)=\begin{cases}0 & T_{\mathrm{mean}}<273.15\\ 1-T_{\mathrm{opt}}^{-2}\left(T_{\mathrm{mean}}-T_{\mathrm{opt}}\right)^{2} & \left(T_{\mathrm{mean}}>T_{\mathrm{opt}}+1\right)\\ & \cup\left(273.15\leq T_{\mathrm{mean}}<T_{\mathrm{opt}}-1\right),\\ 1 & T_{\mathrm{opt}}-1\leq T_{\mathrm{mean}}\leq T_{\mathrm{opt}}+1\end{cases} \tag{B20}$$

where c_{R} is the radiation stress parameter fixed at 100 (Zhou et al., 2006), $D_{0.5}$ is the vapour pressure deficit halfway between 1 and c_{D2} set at 1.5 kPa, c_{D1} is the first vapour pressure parameter set at 3, and c_{D2} is the second vapour pressure stress parameter set at 0.1 (Matsumoto et al., 2008). Optimum temperature T_{opt} [K] is based on elevation a.s.l. Z [m] and latitude ϖ [rad] (Cui et al., 2012):

$$T_{\mathrm{opt}}=302.45-0.003\left(Z-|\varpi|\right). \tag{B21}$$

Graphical representations of the stress functions are presented in Fig. B1. Under unfavourable conditions where at least one of the stress functions equals zero, $r_{\mathrm{s,st}}$ is assumed to be 0.58 d m^{-1} (50 000 s m^{-1}), corresponding to the molecular diffusivity of water vapour through leaf cuticula (Tourula and Heikinheimo, 1998). If i_{LA} is zero, no transpiration is allowed.

B3 Daylength

Daylength N [s] is (Glarner, 2006):

$$N=86\,400\frac{\arccos\left(1-b\right)}{\pi}, \tag{B22}$$

where

$$b = 1 - \tan(\varpi)\tan\left[\beta\cos\left(\frac{n_{ws}\pi}{182.625}\right)\right], \tag{B23}$$

where ϖ is the latitude in radians, β is the obliquity of the ecliptic (0.409 radians), and n_{ws} is the number of days since the winter solstice. Because day length must be between 0 and 86 400 s, b is allowed to vary only between 0 and 2.

Appendix C

Evaporation rates and time scales in January and July

Here we show the evaporation fluxes (Figs. C1 and C2) and their respective mean terrestrial residence time scales (Figs. C2 and C4) in January and July. As expected, the seasonality variation is strong. While transpiration becomes dormant in January in the northern latitudes, it grows to equal tropical evaporation rates in July. In South America, we notice that high transpiration rates are shifted from the dry southeast to the central tropical monsoon climate region. Nevertheless, high transpiration time scales remain in the wet tropics due to compensation from the soil moisture stock. Note that the colour scales in Figs. C2 and C4 in the different time scale are different. Transpiration has the longest time scale, while vegetation has the shortest.

Appendix D

Sensitivity to precipitation

Table D1 provides an overview of the sensitivity of runoff and evaporation fluxes to a uniform 5 % reduction in precipitation. A number of observations can be noted.

ESDD
5, 203–279, 2014

Interception and transpiration – Part 1: STEAM

L. Wang-Erlandsson et al.

First, the mean annual STEAM runoff is clearly more sensitive (−10.95 %) to precipitation reduction compared to evaporation (−1.78 %). Second, among the evaporation fluxes, soil moisture evaporation (−2.95 %) and transpiration (−2.32 %) responded most strongly, whereas the vegetation (−0.89 %) and floor interception (−0.65 %) evaporation fluxes reduced only marginally. This is logical, because interception stocks are already small and depend more on rainfall frequency than rainfall amount. Third, the increase in open water evaporation (+0.25 %) is small, and can be explained by decreases in vegetation interception that translated into increases in available energy for water evaporation in wetlands and rice paddies. Fourth, the relative reduction in snow accumulation (−14.63 %) is high since snow melt is unchanged. Last, the global mean evaporative partitioning is changed only insignificantly towards lower transpiration ratio.

The sensitivity of transpiration is highest over the US, Australia, the subtropical South America and Africa, and other areas that at least during part of the years are water constrained. In the wet tropics, transpiration rates do not react to precipitation reductions. Vegetation interception experiences an insignificant relative decrease, which is highest in the north and highest in the tropics. This is probably caused by a combination of lower original interception rates in the boreal forests, and the relatively higher dependence on high rainfall frequency in the tropical forests.

This uniform perturbation of precipitation forcing indicates that STEAM evaporation is much less sensitive to precipitation than runoff. This can be explained by the fact that evaporation is constrained by potential evaporation, which relates to other factors than just precipitation. In wet regions where soil moisture is close to saturation, any excess precipitation would more likely lead to increase in runoff rather than evaporation. The sensitivity of runoff to precipitation data is also reported in the literature (e.g., Fekete et al., 2004) and supports the view that runoff comparisons will not accurately describe how well land-surface models estimate evaporation when precipitation is uncertain.

ESDD
5, 203–279, 2014

Supplementary material related to this article is available online at http://www.earth-syst-dynam-discuss.net/5/203/2014/esdd-5-203-2014-supplement.pdf.

Acknowledgements. L. Wang-Erlandsson and L. J. Gordon carried out this research by funding from the Swedish Research Council (Vetenskapsrådet). R. J. van der Ent and H. H. G. Savenije were funded by the research program Division for Earth and Life Sciences (ALW), which is financed by the Netherlands Organization for Scientific Research (NWO). We thank Wim Bastiaanssen, Jianzhi Dong, Johan Rockström, Patrick Keys, Jens Heinke, and Bart van den Hurk for valuable discussions during the model development.

References

Allen, R. G., Pruitt, W. O., Wright, J. L., Howell, T. A., Ventura, F., Snyder, R., Itenfisu, D., Steduto, P., Berengena, J., Yrisarry, J. B., Smith, M., Pereira, L. S., Raes, D., Perrier, A., Alves, I., Walter, I., and Elliott, R.: A recommendation on standardized surface resistance for hourly calculation of reference ETo by the FAO56 Penman–Monteith method, Agr. Water Manage., 81, 1–22, doi:10.1016/j.agwat.2005.03.007, 2006. 237

Alton, P., Fisher, R., Los, S., and Williams, M.: Simulations of global evapotranspiration using semiempirical and mechanistic schemes of plant hydrology, Global Biogeochem. Cy., 23, GB4032, doi:10.1029/2009GB003540, 2009. 206, 222, 225, 255

Bagley, J. E., Desai, A. R., West, P. C., and Foley, J. A.: A simple, minimal parameter model for predicting the influence of changing land cover on the land–atmosphere system?, Earth Interact., 15, 1–32, doi:10.1175/2011EI394.1, 2011. 227, 258

Balsamo, G., Pappenberger, F., Dutra, E., Viterbo, P., and van den Hurk, B. J. J. M.: A revised land hydrology in the ECMWF model: a step towards daily water flux prediction in a fully-closed water cycle, Hydrol. Process., 25, 1046–1054, doi:10.1002/hyp.7808, 2011. 209

Bastiaanssen, W. G. M., Cheema, M. J. M., Immerzeel, W. W., Miltenburg, I. J., and Pelgrum, H.: The surface energy balance and actual evapotranspiration of the transboundary Indus Basin estimated from satellite measurements and the ETLook model, Water Resour. Res., 48, W11512, doi:10.1029/2011WR010482, 2012. 212, 215

ESDD
5, 203–279, 2014

Breuer, L., Eckhardt, K., and Frede, H.-G.: Plant parameter values for models in temperate climates, Ecol. Model., 169, 237–293, doi:10.1016/S0304-3800(03)00274-6, 2003. 215, 217

Calder, I., Wright, I., Murdiyarso, D., V, E. S. P. B., and Gifford, C.: A study of evaporation from tropical rain forest – West Java, J. Hydrol., 89, 13–31, doi:10.1016/0022-1694(86)90139-3, 1986. 206

Choudhury, B. J., DiGirolamo, N. E., Susskind, J., Darnell, W. L., Gupta, S. K., and Asrar, G.: A biophysical process-based estimate of global land surface evaporation using satellite and ancillary data, II. Regional and global patterns of seasonal and annual variations, J. Hydrol., 205, 186–204, doi:10.1016/S0022-1694(97)00149-2, 1998. 222, 225, 255

Coenders-Gerrits, A. M. J., van der Ent, R. J., Bogaard, T. A., Wang-Erlandsson, L., Hrachowitz, M., and Savenije, H. H. G.: Uncertainties in transpiration estimates, Nature, 506, E1–E2, doi:10.1038/nature12925, 2014. 206, 222, 255

Cuartas, L. A., Tomasella, J., Nobre, A. D., Hodnett, M. G., Waterloo, M. J., and Múnera, J. C.: Interception water-partitioning dynamics for a pristine rainforest in Central Amazonia: marked differences between normal and dry years, Agr. Forest Meteorol., 145, 69–83, doi:10.1016/j.agrformet.2007.04.008, 2007. 226

Cui, Y. P., Liu, J. Y., Hu, Y. F., Bing, L. F., Tao, F. L., and Wang, J. B.: Estimating and Analyzing the Optimum Temperature for Vegetation Growth in China, Journal of Natural Resources, 27, 281–292, 2012 (in Chinese). 238

Dai, A. and Trenberth, K. E.: Estimates of freshwater discharge from continents: latitudinal and seasonal variations, J. Hydrometeorol., 3, 660–687, doi:10.1175/1525-7541(2002)003<0660:EOFDFC>2.0.CO;2, 2002. 229

de Bruin, H. A. R. and Jacobs, C. M.: Forests and regional-scale processes, Biological Sciences, 324, 393–406, 1989. 232

de Jong, S. M. and Jetten, V. G.: Estimating spatial patterns of rainfall interception from remotely sensed vegetation indices and spectral mixture analysis, Int. J. Geogr. Inf. Sci., 21, 529–545, doi:10.1080/13658810601064884, 2007. 217

Dee, D., Uppala, S., Simmons, A. J., Berrisford, P., Poli, P., Kobayashi, S., Andrae, U., Balmaseda, M., Balsamo, G., Bauer, P., Bechtold, P., Beljaars, A. C. M., van de Berg, L., Bidlot, J., Bormann, N., Delsol, C., Dragani, R., Fuentes, M., Geer, A., Haimberger, L., Healy, S., Hersbach, H., Hólm, E., Isaksen, L., Kållberg, P., Köhler, M., Matricardi, M., McNally, A., Monge-Sanz, B., Morcrette, J.-J., Park, B.-K., Peubey, C., de Rosnay, P., Tavolato, C., Thépaut, J.-N., and Vitart, F.: The ERA-Interim reanalysis: configuration and performance of the

ESDD
5, 203–279, 2014

data assimilation system, Q. J. Roy. Meteor. Soc., 137, 553–597, doi:10.1002/qj.828, 2011. 207

Delzon, S. and Loustau, D.: Age-related decline in stand water use: sap flow and transpiration in a pine forest chronosequence, Agr. Forest Meteorol., 129, 105–119, doi:10.1016/j.agrformet.2005.01.002, 2005. 206

Dirmeyer, P. A., Gao, X., Zhao, M., Guo, Z., Oki, T., and Hanasaki, N.: GSWP-2: multimodel analysis and implications for our perception of the land surface, B. Am. Meteorol. Soc., 87, 1381–1397, doi:10.1175/BAMS-87-10-1381, 2006. 222, 255

Döll, P. and Lehner, B.: Validation of a new global 30 min drainage direction map, J. Hydrol., 258, 214–231, doi:10.1016/S0022-1694(01)00565-0, 2002. 209, 226

FAO/IIASA/ISRIC/ISSCAS/JRC: Harmonized World Soil Database (version 1.2), FAO, Rome, Italy and IIASA, Laxenburg, Austria„ 2012. 209

Feddema, J. J., Oleson, K. W., Bonan, G. B., Mearns, L. O., Buja, L. E., Meehl, G. A., and Washington, W. M.: The importance of land-cover change in simulating future climates, Science, 310, 1674–1678, doi:10.1126/science.1118160, 2005. 233

Feddes, R. A., Hoff, H., Bruen, M., Dawson, T., de Rosnay, P., Dirmeyer, P. A., Jackson, R. B., Kabat, P., Kleidon, A., Lilly, A., and Pitman, A. J.: Modeling root water uptake in hydrological and climate models, B. Am. Meteorol. Soc., 82, 2797–2809, doi:10.1175/1520-0477(2001)082<2797:MRWUIH>2.3.CO;2, 2001. 228

Federer, C., Vörösmarty, C., and Fekete, B.: Intercomparison of methods for calculating potential evaporation in regional and global water balance models, Water Resour. Res., 32, 2315–2321, doi:10.1029/96WR00801, 1996. 215

Fekete, B., Vörösmarty, C., Roads, J., and Willmott, C.: Uncertainties in precipitation and their impacts on runoff estimates, J. Climate, 17, 294–304, doi:10.1175/1520-0442(2004)017<0294:UIPATI>2.0.CO;2, 2004. 230, 240

Fekete, B. M., Vörösmarty, C. J., and Grabs, W.: Global Composite Runoff Fields Based on Observed River Discharge and Simulated Water Balances, Tech. rep., Global Runoff Data Centre, Federal Insititute of Hydrology, Koblenz, 2000. 209, 229

Fenicia, F., Savenije, H. H. G., and Avdeeva, Y.: Anomaly in the rainfall-runoff behaviour of the Meuse catchment. Climate, land-use, or land-use management?, Hydrol. Earth Syst. Sci., 13, 1727–1737, doi:10.5194/hess-13-1727-2009, 2009. 206

Ferretti, D. F., Pendall, E., Morgan, J. A., Nelson, J. A., LeCain, D., and Mosier, A. R.: Partitioning evapotranspiration fluxes from a Colorado grassland using stable isotopes: seasonal variations and ecosystem implications of elevated atmospheric CO_2, Plant Soil, 254, 291–303, doi:10.1023/A:1025511618571, 2003. 205

Forrester, D. I., Collopy, J. J., and Morris, J. D.: Transpiration along an age series of Eucalyptus globulus plantations in southeastern Australia, Forest Ecol. Manag., 259, 1754–1760, doi:10.1016/j.foreco.2009.04.023, 2010. 206

Franken, W., Leopoldo, P. R., Matsui, E., and Ribeiro, M. D. N. G.: Estudo da interceptação da água de chuva na coberta florestal Amazônica do tipo terra firme, Acta Amazonica, 12, 327–331, 1992. 226

Friedl, M. A., Sulla-Menashe, D., Tan, B., Schneider, A., Ramankutty, N., Sibley, A., and Huang, X.: MODIS Collection 5 global land cover: algorithm refinements and characterization of new datasets, Remote Sens. Environ., 114, 168–182, doi:10.1016/j.rse.2009.08.016, 2010. 208

Gao, H., Hrachowitz, M., Fenicia, F., Gharari, S., and Savenije, H. H. G.: Testing the realism of a topography driven model (FLEX-Topo) in the nested catchments of the Upper Heihe, China, Hydrol. Earth Syst. Sci. Discuss., 10, 12663–12716, doi:10.5194/hessd-10-12663-2013, 2013. 228

Gerrits, A. M. J., Savenije, H. H. G., Veling, E. J. M., and Pfister, L.: Analytical derivation of the Budyko curve based on rainfall characteristics and a simple evaporation model, Water Resour. Res., 45, 1–15, doi:10.1029/2008WR007308, 2009. 205

Gerrits, A. M. J., Pfister, L., and Savenije, H. H. G.: Spatial and temporal variability of canopy and forest floor interception in a beech forest, Hydrol. Process., 24, 3011–3025, doi:10.1002/hyp.7712, 2010. 218

Gerten, D., Hoff, H., Bondeau, A., Lucht, W., Smith, P., and Zaehle, S.: Contemporary "green" water flows: simulations with a dynamic global vegetation and water balance model, Phys. Chem. Earth, 30, 334–338, doi:10.1016/j.pce.2005.06.002, 2005. 206, 221, 255

Glarner, H.: Length of Day and Twilight, available at: http://herbert.gandraxa.com/length_of_day.xml (last access: 2 November 2012), 2006. 238

Gordon, L. J., Steffen, W., Jönsson, B. F., Folke, C., Falkenmark, M., and Johannessen, A. s.: Human modification of global water vapor flows from the land surface, P. Natl. Acad. Sci. USA, 102, 7612–7617, doi:10.1073/pnas.0500208102, 2005. 224, 226, 233, 257

Haddeland, I., Clark, D. B., Franssen, W., Ludwig, F., Voß, F., Arnell, N. W., Bertrand, N., Best, M., Folwell, S., Gerten, D., Gomes, S., Gosling, S. N., Hagemann, S., Hanasaki, N., Harding, R., Heinke, J., Kabat, P., Koirala, S., Oki, T., Polcher, J., Stacke, T., Viterbo, P.,

ESDD
5, 203–279, 2014

Interception and transpiration – Part 1: STEAM

L. Wang-Erlandsson et al.

Weedon, G. P., and Yeh, P.: Multimodel estimate of the global terrestrial water balance: setup and first results, J. Hydrometeorol., 12, 869–884, doi:10.1175/2011JHM1324.1, 2011. 206, 221, 230, 233, 259

Harding, R., Best, M., Blyth, E., Hagemann, S., Kabat, P., Tallaksen, L. M., Warnaars, T., Wiberg, D., Weedon, G. P., van Lanen, H., Ludwig, F., and Haddeland, I.: WATCH: current knowledge of the terrestrial global water cycle, J. Hydrometeorol., 12, 1149–1156, doi:10.1175/JHM-D-11-024.1, 2011. 230, 259

Herwitz, S. R.: Interception storage capacities of tropical rainforest canopy trees, J. Hydrol., 77, 237–252, doi:10.1016/0022-1694(85)90209-4, 1985. 218

Jarvis, P.: The interpretation of the variations in leaf water potential and stomatal conductance found in canopies in the field, Philos. T. R. Soc. Lond., 273, 1976. 237

Jasechko, S., Sharp, Z. D., Gibson, J. J., Birks, S. J., Yi, Y., and Fawcett, P. J.: Terrestrial water fluxes dominated by transpiration, Nature, 496, 347–50, doi:10.1038/nature11983, 2013. 206, 222, 225, 255

Jiménez, C., Prigent, C., Mueller, B., Seneviratne, S. I., McCabe, M. F., Wood, E. F., Rossow, W. B., Balsamo, G., Betts, A. K., Dirmeyer, P. A., Fisher, J. B., Jung, M., Kanamitsu, M., Reichle, R. H., Reichstein, M., Rodell, M., Sheffield, J., Tu, K., and Wang, K.: Global intercomparison of 12 land surface heat flux estimates, J. Geophys. Res., 116, 1–27, doi:10.1029/2010JD014545, 2011. 233

Jolly, W. M., Nemani, R., and Running, S. W.: A generalized, bioclimatic index to predict foliar phenology in response to climate, Glob. Change Biol., 11, 619–632, doi:10.1111/j.1365-2486.2005.00930.x, 2005. 215, 216

Keys, P. W., van der Ent, R. J., Gordon, L. J., Hoff, H., Nikoli, R., and Savenije, H. H. G.: Analyzing precipitationsheds to understand the vulnerability of rainfall dependent regions, Biogeosciences, 9, 733–746, doi:10.5194/bg-9-733-2012, 2012. 208

Kleidon, A.: Global datasets of rooting zone depth inferred from inverse methods, J. Climate, 17, 2714–2722, doi:10.1175/1520-0442(2004)017<2714:GDORZD>2.0.CO;2, 2004. 215

Kleidon, A. and Heimann, M.: Assessing the role of deep rooted vegetation in the climate system with model simulations: mechanism, comparison to observations and implications for Amazonian deforestation, Clim. Dynam., 16, 183–199, doi:10.1007/s003820050012, 2000. 228

Kleidon, A. and Renner, M.: A simple explanation for the sensitivity of the hydrologic cycle to surface temperature and solar radiation and its implications for global climate change, Earth Syst. Dynam., 4, 455–465, doi:10.5194/esd-4-455-2013, 2013. 233

Lawrence, D. M., Thornton, P. E., Oleson, K. W., and Bonan, G. B.: The partitioning of evapotranspiration into transpiration, soil evaporation, and canopy evaporation in a GCM: impacts on land–atmosphere interaction, J. Hydrometeorol., 8, 862–880, doi:10.1175/JHM596.1, 2007. 206, 222, 224, 255

Lee, J.-E., Oliveira, R. S., Dawson, T. E., and Fung, I.: Root functioning modifies seasonal climate., P. Natl. Acad. Sci. USA, 102, 17576–81, doi:10.1073/pnas.0508785102, 2005. 228

Matsumoto, K., Ohta, T., Nakai, T., Kuwada, T., Daikoku, K., Iida, S., Yabuki, H., Kononov, A. V., van der Molen, M. K., Kodama, Y., Maximov, T. C., Dolman, A., and Hattori, S.: Responses of surface conductance to forest environments in the Far East, Agr. Forest Meteorol., 148, 1926–1940, doi:10.1016/j.agrformet.2008.09.009, 2008. 216, 237, 238

McNaughton, K. and Jarvis, P.: Predicting effects of vegetation changes on transpiration and evaporation, in: Water deficits and plant growth, edited by: Kozlowski, T., vol. 7 edn., Academic Press, New York, 1–47, 1983. 205, 232

Miguez-Macho, G. and Fan, Y.: The role of groundwater in the Amazon water cycle: 2. Influence on seasonal soil moisture and evapotranspiration, J. Geophys. Res., 117, D15114, doi:10.1029/2012JD017540, 2012. 205, 228

Miralles, D. G., Gash, J. H., Holmes, T. R. H., de Jeu, R. A. M., and Dolman, A.: Global canopy interception from satellite observations, J. Geophys. Res., 115, 1–8, doi:10.1029/2009JD013530, 2010. 222, 225, 232, 255

Mohamed, Y. A.: Impact of the Sudd wetland on the Nile hydroclimatology, Water Resour. Res., 41, W08420, doi:10.1029/2004WR003792, 2005. 230

Mohamed, Y. A., van den Hurk, B. J. J. M., and Savenije, H. H. G.: Moisture recycling over the Nile basin, in: Reducing the Vulnerability of Societies to Water Related Risks at the Basin Scale (Proceedings of the third International Symposium on Integrated Water Resource Management, Bochum, Germany), 18–23 September 2006, IAHS Publ.317, available at: http://www.knmi.nl/publications/fulltexts/iahs_mohamed_etal.pdf (last access: 12 March 2014), 2007. 230

Monteith, J. L.: Evaporation and environment, in: Symp Soc Exp Biol, Vol. 19, chap, The State, 205–234, Cambridge University Press, Swansea, 1965. 211

ESDD
5, 203–279, 2014

Interception and transpiration – Part 1: STEAM

L. Wang-Erlandsson et al.

Moran, M., Scott, R., Keefer, T., Emmerich, W., Hernandez, M., Nearing, G., Paige, G., Cosh, M., and O'Neill, P.: Partitioning evapotranspiration in semiarid grassland and shrubland ecosystems using time series of soil surface temperature, Agr. Forest Meteorol., 149, 59–72, doi:10.1016/j.agrformet.2008.07.004, 2009. 205

Mu, Q., Zhao, M., and Running, S. W.: Improvements to a MODIS global terrestrial evapotranspiration algorithm, Remote Sens. Environ., 115, 1781–1800, doi:10.1016/j.rse.2011.02.019, 2011. 224, 225, 257

Mueller, B. and Seneviratne, S. I.: Evaluation of global observations-based evapotranspiration datasets and IPCC AR4 simulations, Geophys. Res. Lett., 38, L06402, doi:10.1029/2010GL046230, 2011. 233

Mueller, B., Hirschi, M., Jimenez, C., Ciais, P., Dirmeyer, P. A., Dolman, A. J., Fisher, J. B., Jung, M., Ludwig, F., Maignan, F., Miralles, D. G., McCabe, M. F., Reichstein, M., Sheffield, J., Wang, K., Wood, E. F., Zhang, Y., and Seneviratne, S. I.: Benchmark products for land evapotranspiration: LandFlux-EVAL multi-data set synthesis, Hydrol. Earth Syst. Sci., 17, 3707–3720, doi:10.5194/hess-17-3707-2013, 2013. 206, 208, 209, 221

Oishi, A. C., Oren, R., and Stoy, P. C.: Estimating components of forest evapotranspiration: a footprint approach for scaling sap flux measurements, Agr. Forest Meteorol., 148, 1719–1732, doi:10.1016/j.agrformet.2008.06.013, 2008. 206

Oki, T. and Kanae, S.: Global hydrological cycles and world water resources., Science, 313, 1068–72, doi:10.1126/science.1128845, 2006. 220, 229

Pellarin, T., Louvet, S., Gruhier, C., Quantin, G., and Legout, C.: A simple and effective method for correcting soil moisture and precipitation estimates using AMSR-E measurements, Remote Sens. Environ., 136, 28–36, doi:10.1016/j.rse.2013.04.011, 2013. 212

Portmann, F. T., Siebert, S., and Döll, P.: MIRCA2000–Global monthly irrigated and rainfed crop areas around the year 2000: A new high-resolution data set for agricultural and hydrological modeling, Global Biogeochem. Cy., 24, 1–24, doi:10.1029/2008GB003435, 2010. 208

Raz-Yaseef, N., Yakir, D., Schiller, G., and Cohen, S.: Dynamics of evapotranspiration partitioning in a semi-arid forest as affected by temporal rainfall patterns, Agr. Forest Meteorol., 157, 77–85, doi:10.1016/j.agrformet.2012.01.015, 2012. 205

Rockström, J., Gordon, L. J., Folke, C., Falkenmark, M., and Engwall, M.: Linkages among water vapor flows, food production, and terrestrial ecosystem services, Conserv. Ecol., 3, available at: http://www.ecologyandsociety.org/vol3/iss2/art5/, 1999. 224, 257

ESDD
5, 203–279, 2014

Interception and transpiration – Part 1: STEAM

L. Wang-Erlandsson et al.

Rockström, J., Falkenmark, M., Karlberg, L., Hoff, H., Rost, S., and Gerten, D.: Future water availability for global food production: the potential of green water for increasing resilience to global change, Water Resour. Res., 45, W00A12, doi:10.1029/2007WR006767, 2009. 233

Rohwer, J., Gerten, D., and Lucht, W.: Development of Functional Irrigation Types for Improved Global Crop Modelling, Tech. Rep. 104, Potsdam Institute for Climate Impact Research, Potsdam, 2007. 218

Rost, S., Gerten, D., and Heyder, U.: Human alterations of the terrestrial water cycle through land management, Adv. Geosci., 18, 43–50, doi:10.5194/adgeo-18-43-2008, 2008. 226

Rost, S., Gerten, D., Hoff, H., Lucht, W., Falkenmark, M., and Rockström, J.: Global potential to increase crop production through water management in rainfed agriculture, Environ. Res. Lett., 4, 044002, doi:10.1088/1748-9326/4/4/044002, 2009. 233

Savenije, H. H. G.: The importance of interception and why we should delete the term evapotranspiration from our vocabulary, Hydrol. Process., 18, 1507–1511, doi:10.1002/hyp.5563, 2004. 205

Saxton, K. E. and Rawls, W. J.: Soil water characteristic estimates by texture and organic matter for hydrologic solutions, Soil Sci. Soc. Am. J., 70, 1569, doi:10.2136/sssaj2005.0117, 2006. 209

Schlesinger, W. H. and Jasechko, S.: Transpiration in the global water cycle, Agr. Forest Meteorol., 189–190, 115–117, doi:10.1016/j.agrformet.2014.01.011, 2014. 206, 221, 224, 225, 232, 255

Scurlock, J. M. O., Asner, G. P., and Gower, S. T.: Worldwide Historical Estimates of Leaf Area Index, 1932–2000, Tech. Rep. December, Oak Ridge National Laboratory, Tennessee, available at: http://web.ornl.gov/~webworks/cppr/y2002/rpt/112600.pdf (last access: 13 March 2013), 2001. 215

Seckler, D., Amarasinghe, U., Molden, D., de Silva, R., and Barker, R.: World Water Demand and Supply, 1990 to 2025: Scenarios and Issues, Tech. rep., International Water Management Institute (IWMI), Colombo, Sri Lanka, 1998. 226

Shukla, J., Nobre, C., and Sellers, P.: Amazon deforestation and climate change, Science, 247, 1322–1325, doi:10.1126/science.247.4948.1322, 1990. 258

Shuttleworth, W. J.: Evaporation from Amazonian Rainforest, P. Roy. Soc. B-Biol. Sci., 233, 321–346, doi:10.1098/rspb.1988.0024, 1988. 206

Shuttleworth, W. J.: Terrestrial Hydrometeorology, Wiley-Blackwell, West Sussex, 1 Edn., doi:10.1002/9781119951933, 2012. 217, 235

ESDD
5, 203–279, 2014

Interception and transpiration – Part 1: STEAM

L. Wang-Erlandsson et al.

Siebert, S. and Döll, P.: Quantifying blue and green virtual water contents in global crop production as well as potential production losses without irrigation, J. Hydrol., 384, 198–217, doi:10.1016/j.jhydrol.2009.07.031, 2010. 208
Snyder, P., Delire, C., and Foley, J.: Evaluating the influence of different vegetation biomes on the global climate, Clim. Dynam., 23, 279–302, doi:10.1007/s00382-004-0430-0, 2004. 258
Stewart, J.: Modelling surface conductance of pine forest, Agr. Forest Meteorol., 43, 19–35, doi:10.1016/0168-1923(88)90003-2, 1988. 237
Syed, T. H., Famiglietti, J. S., Chambers, D. P., Willis, J. K., and Hilburn, K.: Satellite-based global-ocean mass balance estimates of interannual variability and emerging trends in continental freshwater discharge., P. Natl. Acad. Sci. USA, 107, 17916–17921, doi:10.1073/pnas.1003292107, 2010. 229
Teuling, A. J., Seneviratne, S. I., Stöckli, R., Reichstein, M., Moors, E., Ciais, P., Luyssaert, S., van den Hurk, B. J. J. M., Ammann, C., Bernhofer, C., Dellwik, E., Gianelle, D., Gielen, B., Grünwald, T., Klumpp, K., Montagnani, L., Moureaux, C., Sottocornola, M., and Wohlfahrt, G.: Contrasting response of European forest and grassland energy exchange to heatwaves, Nat. Geosci., 3, 722–727, doi:10.1038/ngeo950, 2010. 205, 232
Tobón Marin, C., Bouten, W., and Sevink, J.: Gross rainfall and its partitioning into throughfall, stemflow and evaporation of intercepted water in four forest ecosystems in western Amazonia, J. Hydrol., 237, 40–57, doi:10.1016/S0022-1694(00)00301-2, 2000. 226
Tourula, T. and Heikinheimo, M.: Modelling evapotranspiration from a barley field over the growing season, Agr. Forest Meteorol., 91, 237–250, doi:10.1016/S0168-1923(98)00065-3, 1998. 238
Trambauer, P., Dutra, E., Maskey, S., Werner, M., Pappenberger, F., van Beek, L. P. H., and Uhlenbrook, S.: Comparison of different evaporation estimates over the African continent, Hydrol. Earth Syst. Sci., 18, 193–212, doi:10.5194/hess-18-193-2014, 2014. 233
Trenberth, K. E., Smith, L., Qian, T., Dai, A., and Fasullo, J. T.: Estimates of the global water budget and its annual cycle using observational and model data, J. Hydrometeorol., 8, 758–769, doi:10.1175/JHM600.1, 2007. 220
Tshimanga, R. M.: Hydrological Uncertainty Analysis and Scenario-Based Streamflow Modelling for the Congo River Basin, Ph.D. thesis, Rhodes University, available at: http://eprints.ru.ac.za/2937/1/TSHIMANGA-PhD-TR12-49.pdf (last access: 12 March 2014), 2012. 230
van den Hoof, C., Vidale, P. L., Verhoef, A., and Vincke, C.: Improved evaporative flux partitioning and carbon flux in the land surface model JULES: impact on the simulation

ESDD
5, 203–279, 2014

of land surface processes in temperate Europe, Agr. Forest Meteorol., 181, 108–124, doi:10.1016/j.agrformet.2013.07.011, 2013. 217, 225, 255

van den Hurk, B. J. J. M.: Impact of leaf area index seasonality on the annual land surface evaporation in a global circulation model, J. Geophys. Res., 108, 4191, doi:10.1029/2002JD002846, 2003. 215

van den Hurk, B. J. J. M., Viterbo, P., Beljaars, A. C. M., and Betts, A. K.: Offline Validation of the ERA40 Surface Scheme, Tech. rep., European Centre for Medium-Range Weather Forecasts (ECMWF), available at: http://www.knmi.nl/publications/fulltexts/tm295.pdf (last access: 12 March 2014), 2000. 215

van der Ent, R. J. and Savenije, H. H. G.: Length and time scales of atmospheric moisture recycling, Atmos. Chem. Phys., 11, 1853–1863, doi:10.5194/acp-11-1853-2011, 2011. 208

van der Ent, R. J., Savenije, H. H. G., Schaefli, B., and Steele-Dunne, S. C.: Origin and fate of atmospheric moisture over continents, Water Resour. Res., 46, 1–12, doi:10.1029/2010WR009127, 2010. 208

van der Ent, R. J., Wang-Erlandsson, L., Keys, P. W., and Savenije, H. H. G.: Contrasting roles of interception and transpiration in the hydrological cycle – Part 2: Moisture recycling, Earth Syst. Dynam. Discuss., 5, 281–326, doi:10.5194/esdd-5-281-2014, 2014. 206

Vinukollu, R. K., Meynadier, R., Sheffield, J., and Wood, E. F.: Multi-model, multi-sensor estimates of global evapotranspiration: climatology, uncertainties and trends, Hydrol. Process., 25, 3993–4010, doi:10.1002/hyp.8393, 2011. 221, 230

Wang, D., Wang, G., and Anagnostou, E. N.: Evaluation of canopy interception schemes in land surface models, J. Hydrol., 347, 308–318, doi:10.1016/j.jhydrol.2007.09.041, 2007. 225

Wang, P., Song, X., Han, D., Zhang, Y., and Zhang, B.: Determination of evaporation, transpiration and deep percolation of summer corn and winter wheat after irrigation, Agr. Water Manage., 105, 32–37, doi:10.1016/j.agwat.2011.12.024, 2012. 205

Wenninger, J., Beza, D. T., and Uhlenbrook, S.: Experimental investigations of water fluxes within the soil–vegetation–atmosphere system: stable isotope mass-balance approach to partition evaporation and transpiration, Phys. Chem. Earth, 35, 565–570, doi:10.1016/j.pce.2010.07.016, 2010. 205

Wilson, K. B., Hanson, P. J., Mulholland, P. J., Baldocchi, D. D., and Wullschleger, S. D.: A comparison of methods for determining forest evapotranspiration and its components: sap-flow, soil water budget, eddy covariance and catchment water balance, Agr. Forest Meteorol., 106, 153–168, doi:10.1016/S0168-1923(00)00199-4, 2001. 206

Zeng, X.: Global vegetation root distribution for land modeling, J. Hydrometeorol., 2, 525–530, doi:10.1175/1525-7541(2001)002<0525:GVRDFL>2.0.CO;2, 2001. 215

Zhang, H., Henderson-Sellers, A., and McGuffie, K.: Impacts of tropical deforestation, Part 1: Process analysis, J. Climate, 9, 1497–1517, doi:10.1175/1520-0442(1996)009<1497:IOTDPI>2.0.CO;2, 1996. 258

Zhou, M., Ishidaira, H., Hapuarachchi, H., Magome, J., Kiem, A., and Takeuchi, K.: Estimating potential evapotranspiration using Shuttleworth–Wallace model and NOAA-AVHRR NDVI data to feed a distributed hydrological model over the Mekong River basin, J. Hydrol., 327, 151–173, doi:10.1016/j.jhydrol.2005.11.013, 2006. 215, 237, 238

Table 1. List of land-use types used in STEAM.

ID	Abbreviation	Full name
1	WAT	Water
2	ENF	Evergreen forest
3	EBF	Evergreen broadleaf forest
4	ENF	Deciduous needle leaf forest
5	DBF	Deciduous broadleaf forest
6	MXF	Mixed forest
7	CSH	Closed shrubland
8	OSH	Open shrubland
9	WSA	Woody savannah
10	SAV	Savannah
11	GRA	Grassland
12	WET	Permanent wetland
13	CRO	Cropland, rainfed
14	URB	Urban and built-up
15	MOS	Crop/natural mosaic
16	ICE	Snow/ice
17	BAR	Barren
18	IRR	Irrigated cropland (other than rice)
19	RIC	Irrigated rice paddies

ESDD
5, 203–279, 2014

Table 2. Fractions of vegetation in soil ϕ_{vs}, vegetation in water ϕ_{vw}, and open water ϕ_{ow} by land-use type.

Land-use type	ϕ_{vs}	ϕ_{vw}	ϕ_{ow}
12:WET	1/3	1/3	1/3
19:RIC	1/10	9/10	0
01:WAT	0	0	1
Other	1	0	0

Discussion Paper | Discussion Paper | Discussion Paper | Discussion Paper |

ESDD
5, 203–279, 2014

Interception and transpiration – Part 1: STEAM

L. Wang-Erlandsson et al.

Title Page
Abstract
Introduction
Conclusions
References
Tables
Figures
◀|
|▶
◀
▶
Back
Close
Full Screen / Esc
Printer-friendly Version
Interactive Discussion

Table 3. Land-use parameters used in STEAM. See Table 1 for a complete list of the land-use type abbreviations.

Land-use class	$i_{LA,max}$	$i_{LA,min}$	y_{uz}	α	h_{max}	h_{min}	$z_{0,f}$	$r_{s,\,st,\,min}$
Unit	–	–	m	–	m	m	m	$s\,m^{-1}$ [a]
01: WAT	0	0	0	0.08	0	0	0.00137	0
02: ENF	5.5	2	2	0.15	17	17	0.02	300
03: EBF	5.5	2	2	0.18	30	30	0.02	200
04: DNF	5	1	2	0.18	17	17	0.02	300
05: DBF	5.5	1	2	0.18	25	25	0.02	200
06: MXF	5	1	2	0.18	20	20	0.02	250
07: CSH	1.5	0.5	2	0.2	1.5	1.5	0.02	200
08: OSH	1.5	0.5	2	0.2	1	1	0.02	200
09: WSA	2	0.5	2	0.2	0.8	0.8	0.02	150
10: SAV	2	0.5	3.5	0.2	0.8	0.1	0.02	150
11: GRA	2	0.5	1.5	0.2	0.8	0.05	0.01	150
12: WET	4	1	1.5	0.15	1	0.05	0.01	150
13: CRP	3.5	0.5	1.5	0.2	0.8	0.05	0.005	150
14: URB	1	0.1	0.5	0.18	0.8	0	0.001	250
15: MOS	3.5	0.5	1.5	0.2	0.8	0.1	0.005	150
16: ICE	0	0	0	0.7	0	0	0.001	0
17: BAR	0.1	0.01	1.5	0.25	0.8	0	0.001	200
18: IRR	3.5	3.5	0.5	0.2	0.8	0.8	0.005	150
19: RIC	3.5	3.5	0.5	0.2	0.8	0.8	0.005	150

[a] The unit for $r_{s,\,st,\,min}$ is $d\,m^{-1}$ throughout the paper, and only given as $s\,m^{-1}$ in this table to facilitate comparison with other studies.

ESDD
5, 203–279, 2014

Table 4. Overview of global evaporative partitioning estimates.

	E_t	E_v	$(E_f + E_{sm})$	Source
Unit		% of E		
Land-surface models				
STEAM	59	21	16	This study
JULES (with SiB or SPA scheme)	38–48			(Alton et al., 2009)
CLM3	44	17	39	(Lawrence et al., 2007)
LPJ	65			(Gerten et al., 2005)
A biophysical process-based model	52	20	28	(Choudhury et al., 1998)
Other methods				
Literature	61			(Schlesinger and Jasechko, 2014)
Isotope + literature	35–80			(Coenders-Gerrits et al., 2014)
Isotope + literature	80–90			(Jasechko et al., 2013)
Satellite	80	11	7	(Miralles et al., 2010) as cited in (van den Hoof et al., 2013)
Multimodel, GSWP2	48	16	36	(Dirmeyer et al., 2006)

ESDD
5, 203–279, 2014

Table 5. Evaporation partitioning by land-use type, 1999–2008. Symbols are explained in Appendix A.

Land use	Area	P	E	E_v	E_f	E_t	E_{sm}	E_w	E_v	E_f	E_t	E_{sm}	E_w	E_v
Unit	1000 km^2	mm year^{-1}							% of E					% of P
01: WAT	1071	937	1148	0	0	0	0	1148	0	0	0	0	100	0
02: ENF	3224	853	496	154	73	248	21	0	31	15	50	4	0	18
03: EBF	13 541	2542	1208	452	92	651	13	0	37	8	54	1	0	18
04: DNF	1341	481	365	94	66	191	14	0	26	18	52	4	0	20
05: DBF	1350	1057	853	179	83	543	48	0	21	10	64	6	0	17
06: MXF	9349	958	604	158	79	344	22	0	26	13	57	4	0	16
07: CSH	99	554	499	54	57	324	63	0	11	11	65	13	0	10
08: OSH	21 207	432	280	38	43	162	37	0	14	15	58	13	0	9
09: WSA	10 585	1210	733	103	89	494	48	0	14	12	67	6	0	9
10: SAV	9904	1122	860	102	91	601	66	0	12	11	70	8	0	9
11: GRA	18 253	616	393	54	66	241	33	0	14	17	61	8	0	9
12: WET	1218	1151	957	113	26	296	8	514	12	3	31	1	54	10
13: CRP	(10 352–10 851)[a]	789	576	98	23	416	39	0	17	4	72	7	0	12
14: URB	454	991	464	46	42	256	121	0	10	9	55	26	0	5
15: MOS	(7790–7814)[a]	1262	777	165	78	509	25	0	21	10	65	3	0	13
16: ICE	2710	560	30	0	30	0	0	0	0	100	0	0	0	0
17: BAR	18 943	90	57	1	11	20	25	0	1	19	36	44	0	1
18: IRR	(1060–1195)[a]	727	1375	271	80	910	115	0	20	6	66	8	0	37
19: RIC	(175–570)[a]	1453	1457	241	7	545	4	661	17	0	37	0	45	17
Global	133 146	888	555	115	58	326	33	24	59	10	21	6	4	13

[a] Area varies because a monthly varying irrigation map is applied.

ESDD
5, 203–279, 2014

Table 6. Evaporation of lumped land-use types in comparison with other studies.

	STEAM, Year 1999–2008		Gordon et al. (2005)		Schlesinger and Jasechko (2014) based on Mu et al. (2011)	Rockström et al. (1999)
	Area	Average E	Area	Average E	Average E	Average E
Unit	1000 km^2	[mm year^{-1}]	1000 km^2	[mm year^{-1}]	[mm year^{-1}]	[mm year^{-1}]
Forest[a]	28 805	875	46 665	660		
Evergreen needleleaf	3224	496	2134	510	458[e]	487[i]
Evergreen broadleaf	13 541	1206	16 278	1146	1076	1245
Deciduous needleleaf	1341	365		293–795[d]	458[e]	
Deciduous broadleaf	1350	853		293–795[d]	549[f]	729–792[d]
Mixed	9349	604	14 222	313		
Savannah	20 489	733–860[b]	19 562	556		416[j]/882/1267[k]
Shrubland	21 306	280–499[c]	18 649	227	302[g]	270[l]
Grassland	18 253	393	14 393	258	332–583[h]	410[m]

[a] Includes all forest types.
[b] Woody savannah and savannah.
[c] Closed shrubland and open shrubland.
[d] Deciduous forests in general.
[e] Temperate coniferous forest.
[f] Temperate deciduous forest.
[g] Mediterranean shrubland.
[h] Temperate and tropical grassland.
[i] Coniferous forest in general.
[j] Woody savannah.
[k] Wet savannah.
[l] Dry shrubland.
[m] Cool grassland.

ESDD
5, 203–279, 2014

Interception and transpiration – Part 1: STEAM

L. Wang-Erlandsson et al.

Table 7. Influence of deforestation on evaporation.

Model and study	Mean decrease in evaporation [mm year^{-1}]	Area
STEAM (this study)	−457 (Decrease from 1208 mm year^{-1})	Current EBF regions (14 × 106 km^2)
PEGASUS (Bagley et al., 2011)	−447 (−35 W m^{-2})	Amazon
CCM3–IBIS (Snyder et al., 2004)	−388 (−30.4 W m^{-2})	All tropical regions (23 × 106 km^2)
(Shukla et al., 1990)	−496 (Decrease from 1657 mm year^{-1})	Amazon
CCM1–BATS (Zhang et al., 1996)	−222 (Decrease from 1243 mm year^{-1})	Amazon basin

ESDD
5, 203–279, 2014

Table 8. Comparison of STEAM output (1999–2008) with evaporation and runoff provided by the WaterMIP (Water Model Intercomparison Project) (1985–1999) (Haddeland et al., 2011; Harding et al., 2011). The ERA-I precipitation used to force STEAM and the WFD (Watch Forcing Data) precipitation used to force WaterMIP are also shown for each compared river basin.

	E_{STEAM}	$E_{WaterMIP}$			Q_{STEAM}	$Q_{WaterMIP}$			$P_{ERA\text{-}I}$	P_{WFD}
		Low	Mean	High		Low	Mean	High		
Unit	mm year^{-1}									
Amazon	1154	1021	1195	1430	1228	815	1043	1207	2382	2243
Mississippi	595	492	642	747	93	167	269	418	692	909
Ganges/Brahmaputra	737	410	546	828	811	553	891	1038	1555	1447
Lena	318	172	230	283	149	103	151	211	487	385
Global	555	415	499	586	325	290	375	457	888	872

Discussion Paper | Discussion Paper | Discussion Paper | Discussion Paper |

ESDD

5, 203–279, 2014

Interception and transpiration – Part 1: STEAM

L. Wang-Erlandsson et al.

Table A1. List of symbols.

Symbol	Units	Description
α	–	Albedo
β	rad	the obliquity of the ecliptic, 0.409 rad
γ	$\mathrm{kPa\,K^{-1}}$	Psychrometric constant
Δn	h	Time step, 24 h
Δt	h	Time step, 3 h
δ	$\mathrm{kPa\,K^{-1}}$	Slope of the saturated vapour pressure curve
η_{clay}	%	Clay content of the top soil
Θ_{top}	–	Effective saturation of top soil
θ_{uz}	–	Volumetric soil moisture content of the unsaturated zone
$\theta_{\mathrm{uz,\,fc}}$	–	Volumetric soil moisture content at field capacity in the unsaturated zone
θ_{top}	–	Volumetric soil moisture content of top soil
$\theta_{\mathrm{top,\,sat}}$	–	Volumetric soil moisture content of top soil at saturation
$\theta_{\mathrm{top,\,res}}$	–	Volumetric soil moisture content of top soil at residual point
$\theta_{\mathrm{uz,\,wp}}$	–	Volumetric soil moisture content at wilting point
κ	–	Von Kármán constant, 0.41.
λ	$\mathrm{MJ\,kg^{-1}}$	Latent heat of vaporisation of water
ξ_{mw}	–	Ratio of the molecular weight of water vapour to that for dry air, 0.622.
ρ_{a}	$\mathrm{kg\,m^{-3}}$	Density of air.
ρ_{w}	$\mathrm{kg\,m^{-3}}$	Density of water
τ_{ts}	day	Mean terrestrial time scale
ϕ_{lu}	–	Land-use fraction
ϕ_{ow}	–	Open water fraction
ϕ_{vw}	–	Vegetation in water fraction
ϕ_{vs}	–	Vegetation in soil fraction
χ	h	Top soil moisture dry out time parameter
χ_{min}	h	Minimum top soil moisture dry out time parameter, 60 h.
ω	rad	Latitude
C_p	$\mathrm{MJ\,kg^{-1}\,K^{-1}}$	Heat capacity of water at constant pressure, $1.01\times10^{-3}\ \mathrm{MJ\,kg^{-1}\,K^{-1}}$

ESDD
5, 203–279, 2014

Interception and transpiration – Part 1: STEAM

L. Wang-Erlandsson et al.

Table A1. Continued.

Symbol	Units	Description
c_{AR}	–	Area reduction factor, 0.4
c_{D1}	–	Vapor pressure stress parameter, 3.
c_{D2}	–	Vapor pressure stress parameter, 0.1.
c_{R}	–	Radiation stress parameter, 100.
c_{sc}	–	Storage capacity factor, 0.2.
c_{uz}	–	Soil moisture stress parameter, 0.07
$D_{0.5}$	kPa	Vapour pressure deficit coefficient, 1.5 kPa
D_{a}	kPa	Vapour pressure deficit
d	m	Zero plane displacement
E	$\mathrm{m\,d^{-1}}$	Total evaporation
E_{f}	$\mathrm{m\,d^{-1}}$	Floor interception evaporation
$E_{f,\,lu,\,vs}$	$\mathrm{m}\ (\Delta t)^{-1}$	Land-use specific floor interception evaporation in ϕ_{vs}
E_{p}	$\mathrm{m}\ (\Delta t)^{-1}$	Potential evaporation
$E_{p,\,day}$	$\mathrm{m\,d^{-1}}$	Potential evaporation
E_{sm}	$\mathrm{m\,d^{-1}}$	Soil moisture evaporation
$E_{sm,\,lu,\,vs}$	$\mathrm{m}\ (\Delta t)^{-1}$	Land-use specific soil moisture evaporation in ϕ_{vs}
E_{t}	$\mathrm{m\,d^{-1}}$	Transpiration evaporation
$E_{t,\,lu,\,vs}$	$\mathrm{m}\ (\Delta t)^{-1}$	Land-use specific transpiration in ϕ_{vs}
$E_{t,\,lu,\,vw}$	$\mathrm{m}\ (\Delta t)^{-1}$	Land-use specific transpiration in ϕ_{vw}
E_{v}	$\mathrm{m\,d^{-1}}$	Vegetation interception evaporation
$E_{v,\,lu,\,vs}$	$\mathrm{m}\ (\Delta t)^{-1}$	Land-use specific vegetation interception evaporation in ϕ_{vs}
$E_{v,\,lu,\,vw}$	$\mathrm{m}\ (\Delta t)^{-1}$	Land-use specific vegetation interception evaporation in ϕ_{vw}
E_{w}	$\mathrm{m\,d^{-1}}$	Open water evaporation
$E_{w,\,lu,\,ow}$	$\mathrm{m}\ (\Delta t)^{-1}$	Land-use specific water evaporation in ϕ_{ow}
$E_{w,\,lu,\,vw}$	$\mathrm{m}\ (\Delta t)^{-1}$	Land-use specific open water evaporation in ϕ_{ow}
e_{a}	kPa	Actual vapor pressure
e_{s}	kPa	Saturated vapor pressure
h	m	Plant height
h_{max}	m	Minimum plant height

ESDD
5, 203–279, 2014

Interception and transpiration – Part 1: STEAM

L. Wang-Erlandsson et al.

Table A1. Continued.

Symbol	Units	Description
h_{min}	m	Maximum plant height
I_f	$m\,d^{-1}$	Irrigation applied to S_f
I_g	$m\,d^{-1}$	Gross irrigation
I_{req}	$m\,(\Delta t)^{-1}$	Irrigation requirement
I_{uz}	$m\,d^{-1}$	Irrigation applied to S_{uz}
I_v	$m\,d^{-1}$	Irrigation applied to S_v
i_{GS}	–	Growing Season Index
i_{LA}	$m^2\,m^{-2}$	Leaf Area Index
$i_{LA,eff}$	$m^2\,m^{-2}$	Effective Leaf Area Index
$i_{LA,max}$	$m^2\,m^{-2}$	Maximum Leaf Area Index
$i_{LA,min}$	$m^2\,m^{-2}$	Minimum Leaf Area Index
J_{add}	$m\,(\Delta t)^{-1}$	Water added in water stores to compensate for lack of horizontal flows
k	–	Function of r_a and r_s
N	s	Day length
N_{high}	s	Day length, higher sub-optimal threshold, assumed to be 39 600 s.
N_{low}	s	Day length, lower sub-optimal threshold, assumed to be 36 000 s.
n_{ws}	day	Number of days since winter solstice
p	kPa	atmospheric pressure
P	$m\,d^{-1}$	Total precipitation
P_{eff}	$m\,d^{-1}$	Effective precipitation, (i.e., overflow from floor interception stock to unsaturated zone stock)
P_{melt}	$m\,d^{-1}$	Snowmelt
P_{rf}	$m\,(\Delta t)^{-1}$	Rainfall
P_{sf}	$m\,(\Delta t)^{-1}$	Snowfall
P_{tf}	$m\,(\Delta t)^{-1}$	Throughfall, (i.e., overflow from vegetation interception stock to floor interception stock)
Q_{uz}	$m\,(\Delta t)^{-1}$	Outlow from S_{uz}
Q_w	$m\,(\Delta t)^{-1}$	Runoff from S_w
r_a	$d\,m^{-1}$	Aerodynamic resistance
$r_{a,f}$	$d\,m^{-1}$	Floor aerodynamic resistance
$r_{a,v}$	$d\,m^{-1}$	Vegetation aerodynamic resistance
$r_{a,w}$	$d\,m^{-1}$	Open water aerodynamic resistance

ESDD
5, 203–279, 2014

Table A1. Continued.

Symbol	Units	Description
r_{s}	$d\,m^{-1}$	Surface resistance
$r_{s,\,sm}$	$d\,m^{-1}$	Surface soil moisture resistance
$r_{s,\,sm,\,min}$	$d\,m^{-1}$	Minimum surface soil moisture resistance
$r_{s,\,st}$	$d\,m^{-1}$	Surface stomatal resistance
$r_{s,\,st,\,min}$	$d\,m^{-1}$	Minimum surface stomatal resistance
R_{net}	$MJ\,m^{-2}\,d^{-1}$	Net radiation
$R_{net,\,lw}$	$MJ\,m^{-2}\,d^{-1}$	Net long wave radiation
R_{sw}	$MJ\,m^{-2}\,d^{-1}$	Short wave radiation
S_{f}	m	Floor interception stock
$S_{f,\,lu}$	m	Floor interception stock of a specific land-use type
$S_{f,\,max}$	m	Floor interception storage capacity
S_{snow}	m	Snow stock
S_{uz}	m	Unsaturated stock
$S_{uz,\,lu}$	m	Unsaturated stock of a specific land-use type
$S_{uz,\,max}$	m	Unsaturated storage capacity
$S_{uz,\,sm}$	m	Unsaturated stock available for soil moisture evaporation
$S_{uz,\,t}$	m	Unsaturated stock available for transpiration
S_{v}	m	Vegetation interception stock
$S_{v,\,lu}$	m	Vegetation interception stock of a specific land-use type
$S_{v,\,max}$	m	Vegetation interception storage capacity
S_{w}	m	Water stock
$S_{w,\,lu}$	m	Water stock of a specific land-use type

Discussion Paper | Discussion Paper | Discussion Paper | Discussion Paper |
ESDD
5, 203–279, 2014
Interception and transpiration – Part 1: STEAM
L. Wang-Erlandsson et al.

Table A1. Continued.

Symbol	Units	Description
T_{dew}	K	Dew point temperature
T_{mean}	K	Daily mean temperature
T_{min}	K	Daily minimum temperature
$T_{min, high}$	K	Daily minimum temperature, higher sub-optimal threshold, 278.15 K.
$T_{min, low}$	K	Daily minimum temperature, lower sub-optimal threshold, 271.15 K.
T_{opt}	K	Optimum photosynthesis temperature
u_{10}	$m\,d^{-1}$	Wind speed at 10 m height
u_{200}	$m\,d^{-1}$	Wind speed at 200 m height
u_{ref}	$m\,d^{-1}$	Wind speed at reference height
y_{uz}	m	Depth of the unsaturated zone
y_{top}	m	Depth of the top soil
Z	m	Elevation
z_0	m	Aerodynamic roughness length
$z_{0,f}$	m	Roughness length of substrate floor
z_{10}	m	Height of wind speed u_{10}
z_{200}	m	Height of wind speed u_{200}
z_{ref}	m	Reference height

Discussion Paper | Discussion Paper | Discussion Paper | Discussion Paper |
ESDD
5, 203–279, 2014
Interception and transpiration – Part 1: STEAM
L. Wang-Erlandsson et al.

Table D1. Overview of the sensitivity of runoff, evaporation, and model snow accumulation to uniform reduction in precipitation quantity, (global mean for 1999–2008).

Flux	Default		5 % reduction in P		Change
	$km^3\,year^{-1}$	% E	$km^3\,year^{-1}$	% E	%
P	118 236	–	112 324	–	−5
Q	43 314	–	38 572	–	−10.95
E	73 835	100	72 524	100	−1.78
E_t	43 346	58.7	42 342	58.4	−2.32
E_v	15 252	20.7	15 116	20.8	−0.89
E_f	7662	10.4	7,612	10.5	−0.65
E_{sm}	4345	5.9	4217	5.8	−2.95
E_w	3229	4.4	3237	4.5	+0.25
dS_{snow}/dt	1087	–	928	–	−14.63

ESDD
5, 203–279, 2014

Interception and transpiration – Part 1: STEAM

L. Wang-Erlandsson et al.

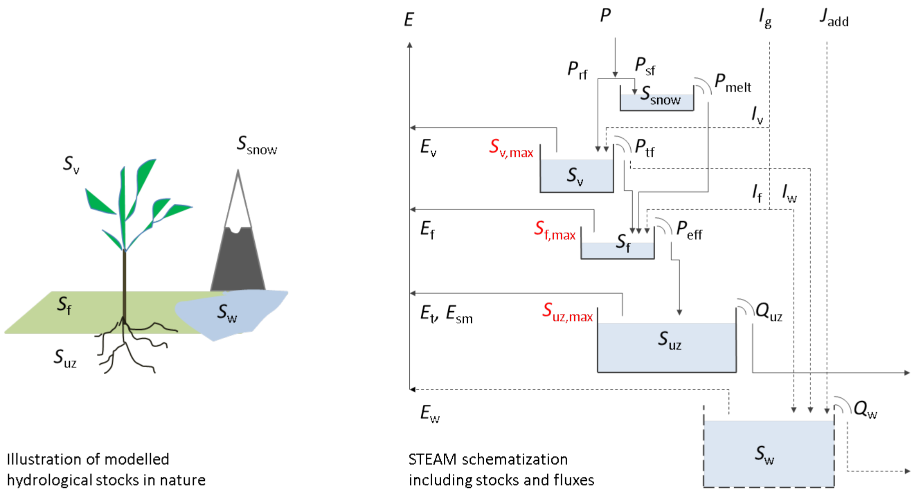

Fig. 1. Water fluxes and stocks in STEAM. Arrows indicate fluxes, and boxes indicate stocks. Dashed lines indicate fluxes and stocks that only exist for particular land-use types. Symbols are listed in Appendix A.

Discussion Paper | Discussion Paper | Discussion Paper | Discussion Paper

ESDD
5, 203–279, 2014

Interception and transpiration – Part 1: STEAM

L. Wang-Erlandsson et al.

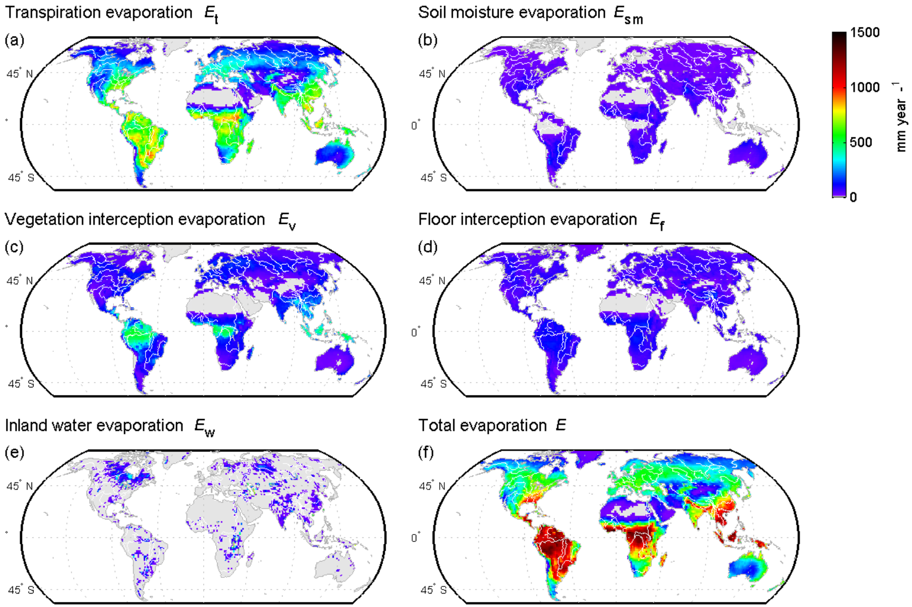

Fig. 2. Mean annual evaporation as estimated by STEAM (1999–2008). Grey indicates areas where the evaporative flux is zero.

ESDD
5, 203–279, 2014

Interception and transpiration – Part 1: STEAM

L. Wang-Erlandsson et al.

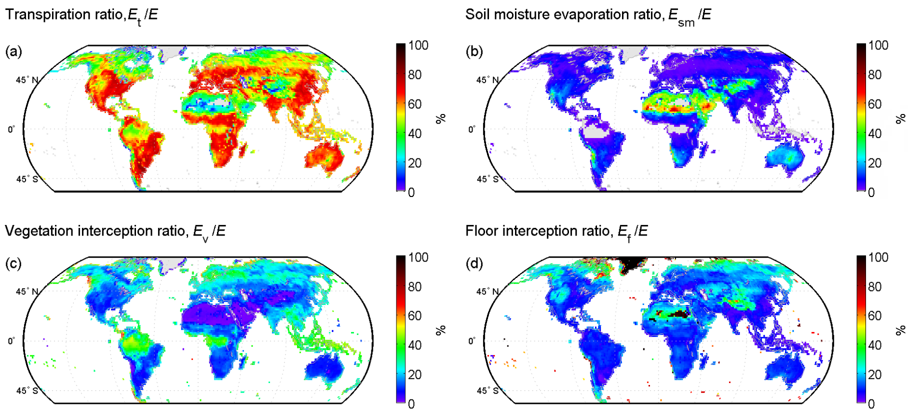

Fig. 3. Partitioned evaporation fluxes expressed as a percentage of total mean annual evaporation (1999–2008). Grey indicates areas where evaporation percentage is zero.

ESDD
5, 203–279, 2014

Interception and transpiration – Part 1: STEAM

L. Wang-Erlandsson et al.

Title Page
Abstract Introduction
Conclusions References
Tables Figures
◀ ▶
Back Close
Full Screen / Esc
Printer-friendly Version
Interactive Discussion

ESDD
5, 203–279, 2014

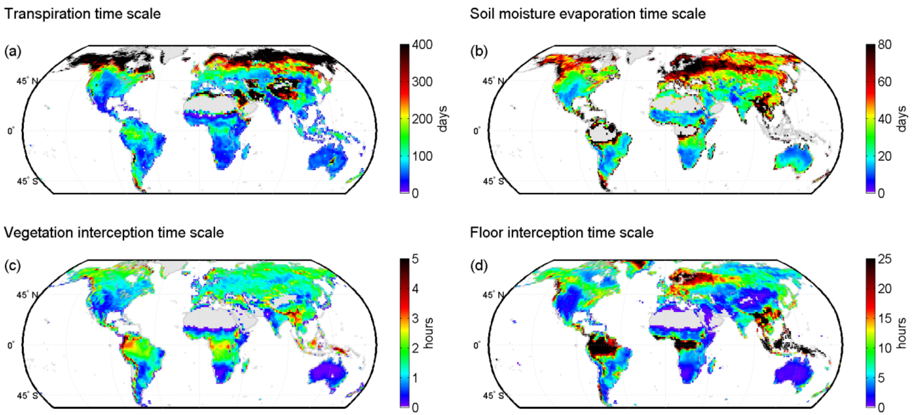

Fig. 4. Average surface time scales of different evaporation fluxes: **(a)** transpiration, **(b)** soil moisture evaporation, **(c)** vegetation interception, and **(d)** floor interception (1999–2008). Grey indicates grid cells with mean evaporation rates below 0.01 mm d^{-1}. Note that the units are in hours for E_v and E_f, and in days for E_t and E_{sm}, see Eq. (26).

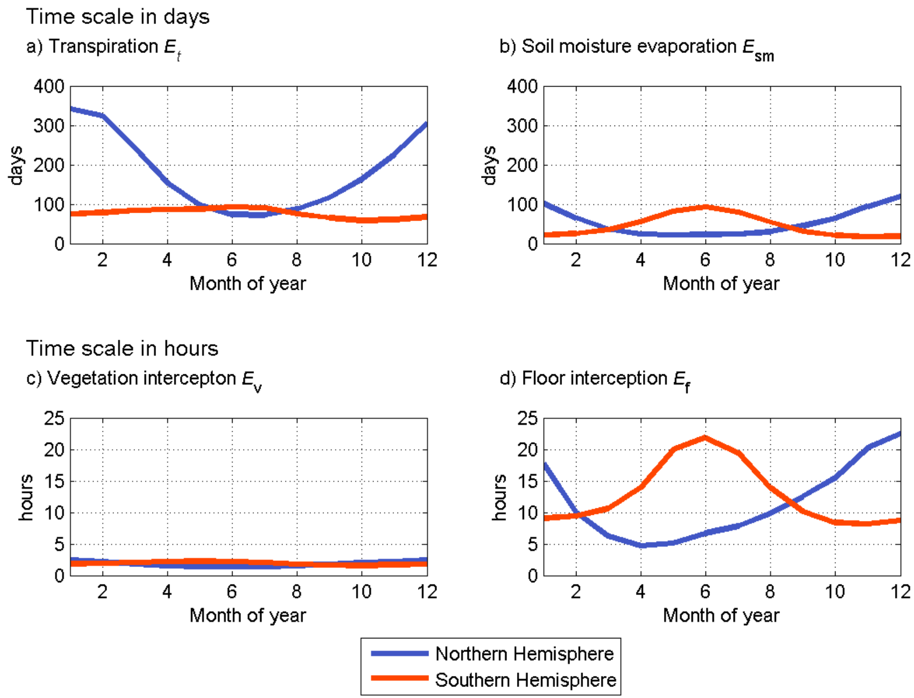

Fig. 5. Changes in time scales over the year for the Northern and Southern Hemisphere.

ESDD
5, 203–279, 2014

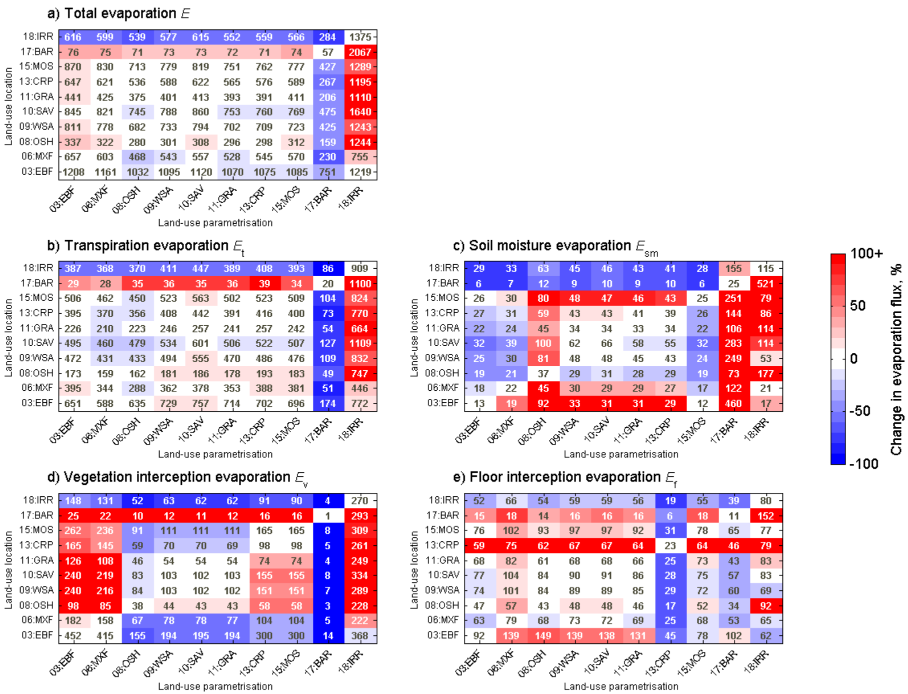

Fig. 6. Mean change in evaporation fluxes in case of land-use swap, 1999–2008. Y axes represent the location of current land use, x axes represent the land-use parametrisation applied. Thus, the diagonal values in white represent the original evaporation flux without any land-use change. Numbers in the matrix represent the evaporation in mm year^{-1}, and the colour represent the relative change in %. As an example, **(a)** shows that the original evaporation is 1208 mm year^{-1} in evergreen broadleaf forest (03:EBF), but applying barren land (17:BAR) parametrisation in those grid cells decreases the total evaporation to 751 mm year^{-1}, which is a 38 % decrease and therefore coloured in blue. See Table 1 for a complete list of the land-use type abbreviations.

ESDD
5, 203–279, 2014

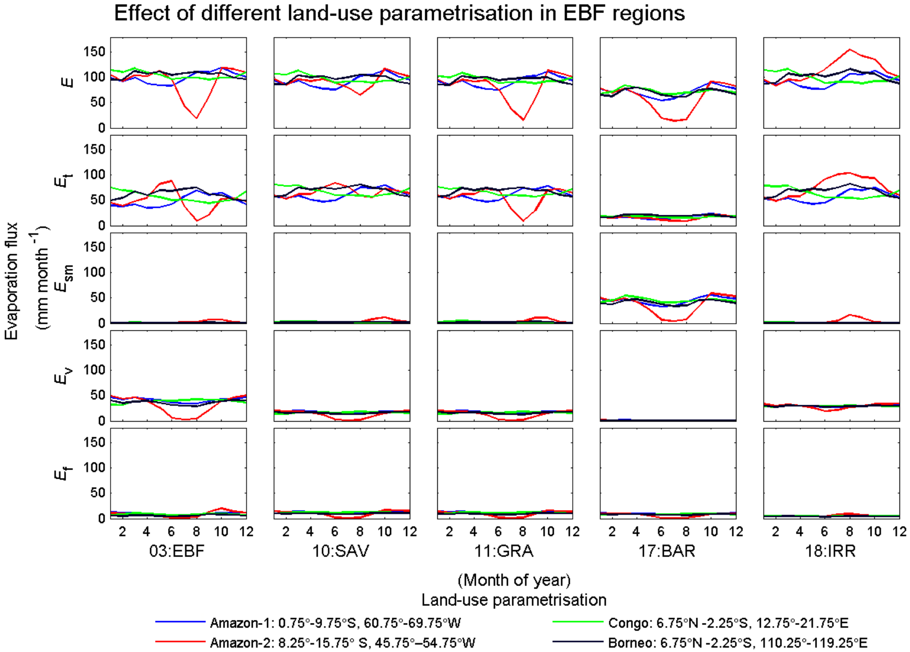

Fig. 7. Mean monthly evaporation when applying different land-use parametrisation in different evergreen broadleaf forest regions. The monthly evaporation for the different evaporation fluxes is represented on the *y* axes, and the land-use parametrisation used is represented on the *x* axes. Thus, the first column of plots represent original evaporation, the second column represent evaporation fluxes using savannah parameters, the third column the grassland parameters, the fourth column the barren land parameters, and the last column the irrigated parametrisation (see Table 3).

ESDD
5, 203–279, 2014

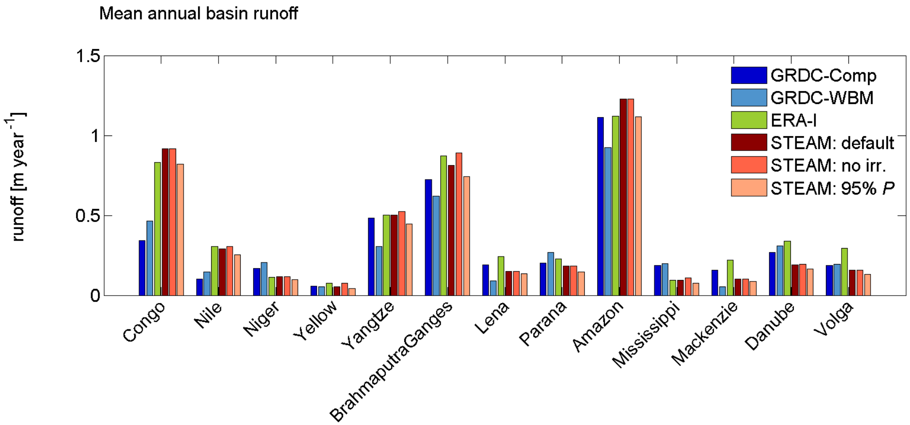

Fig. 8. Mean annual runoff of STEAM compared to other datasets (described in Sect. 2.3). GRDC-Comp (Global Runoff Data Centre composite runoff fields) is the GRDC-WBM (Water Balance Model) runoff corrected using inter-station discharge data. STEAM is run with three settings: with default settings (STEAM: default), with irrigation module switched off (STEAM: no irr) and with 5 % uniform in precipitation forcing (STEAM: 95 % P). STEAM runoff ($\overline{P} - \overline{E} - (\overline{\mathrm{d}S\mathrm{snow}/\mathrm{d}t})$) and ERA-I runoff are for the years 1999–2008. GRDC-Comp and GRDC-WBM represent longterm runoff.

ESDD
5, 203–279, 2014
Interception and transpiration – Part 1: STEAM
L. Wang-Erlandsson et al.

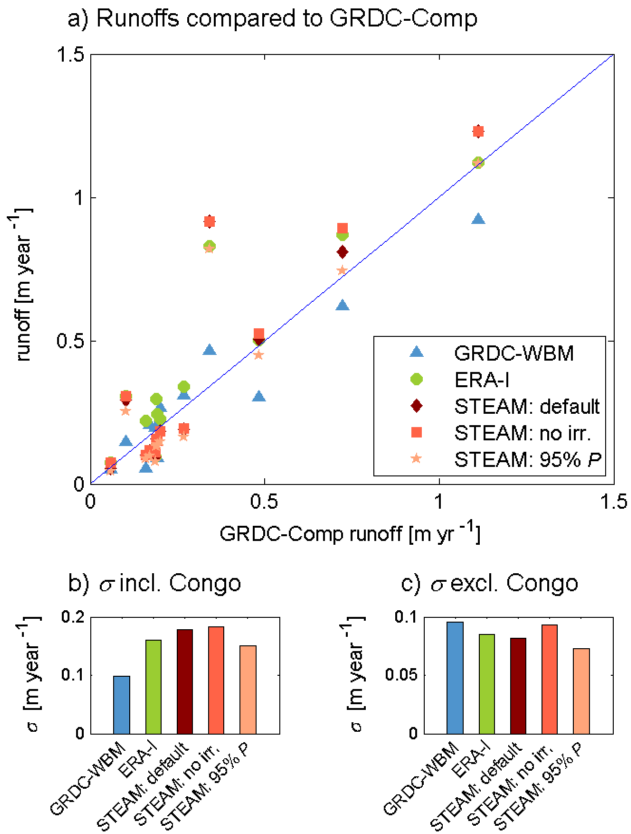

Fig. 9. Comparison between GRDC-Comp (which we consider the benchmark runoff) and the GRDC-WBM, ERA-I, and STEAM runoffs. **(a)** shows the 1 : 1 agreement line; **(b)** shows the standard deviations σ of GRDC-WBM, ERA-I, and STEAM river basin runoff to GRDC-Comp when Congo is included, and **(c)** shows the standard deviations when Congo is excluded.

ESDD
5, 203–279, 2014

Interception and transpiration – Part 1: STEAM

L. Wang-Erlandsson et al.

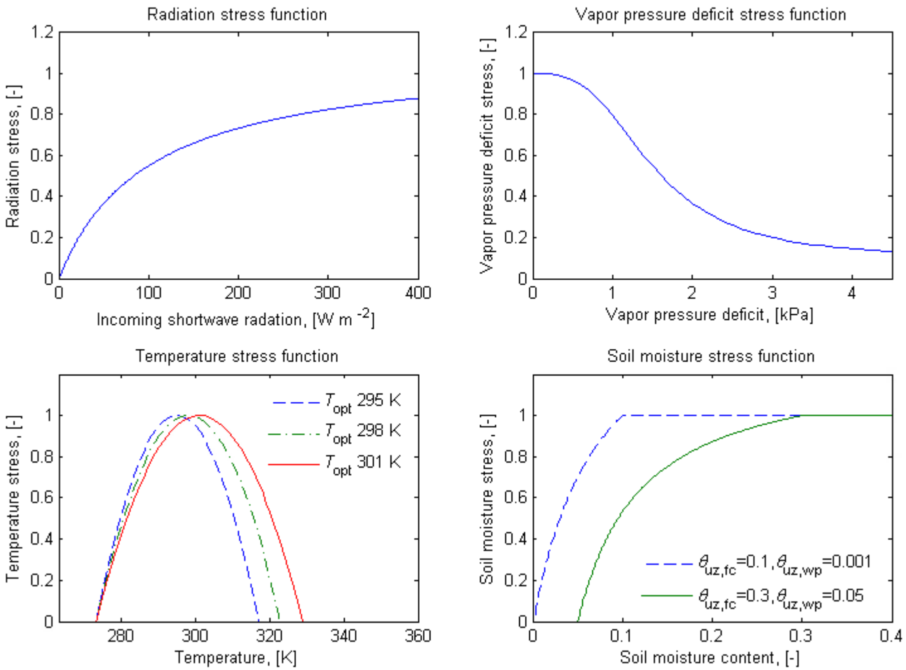

Fig. B1. Stress functions used in the Jarvis–Stewart equation (See Eq. B16.).

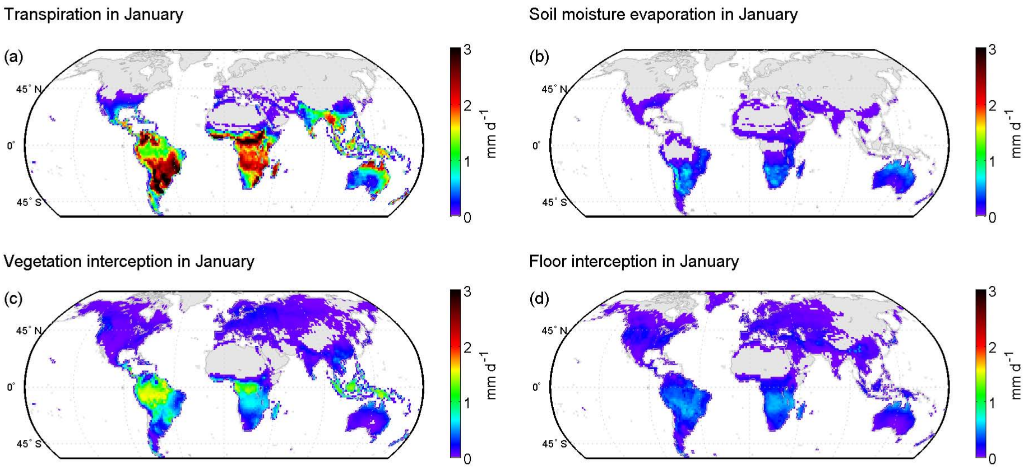

Fig. C1. Mean evaporation rates for the month of January. Grey indicates grid cells with evaporation rates below 0.01 $\text{mm}\,\text{d}^{-1}$.

ESDD
5, 203–279, 2014

Interception and transpiration – Part 1: STEAM

L. Wang-Erlandsson et al.

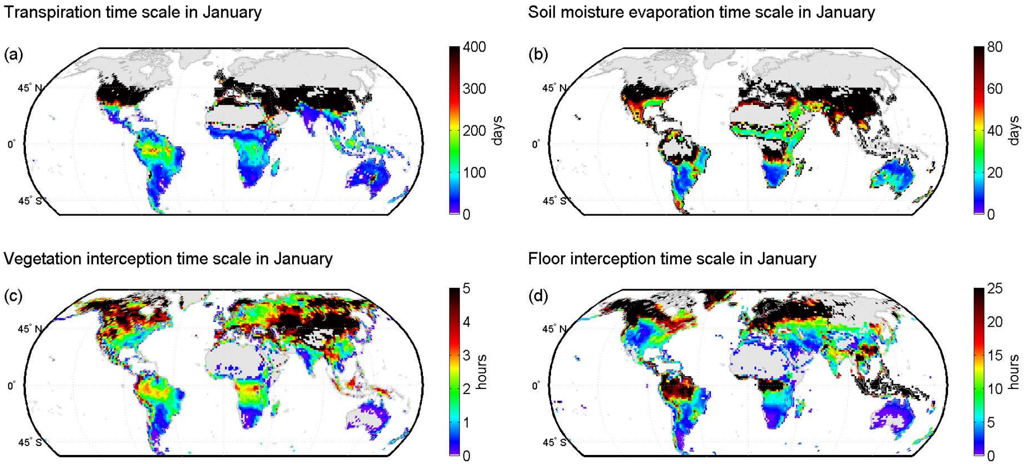

Fig. C2. Mean evaporation time scale for the month of January. Grey indicates grid cells with evaporation rates below 0.01 $mm\,d^{-1}$.

ESDD
5, 203–279, 2014

Interception and transpiration – Part 1: STEAM

L. Wang-Erlandsson et al.

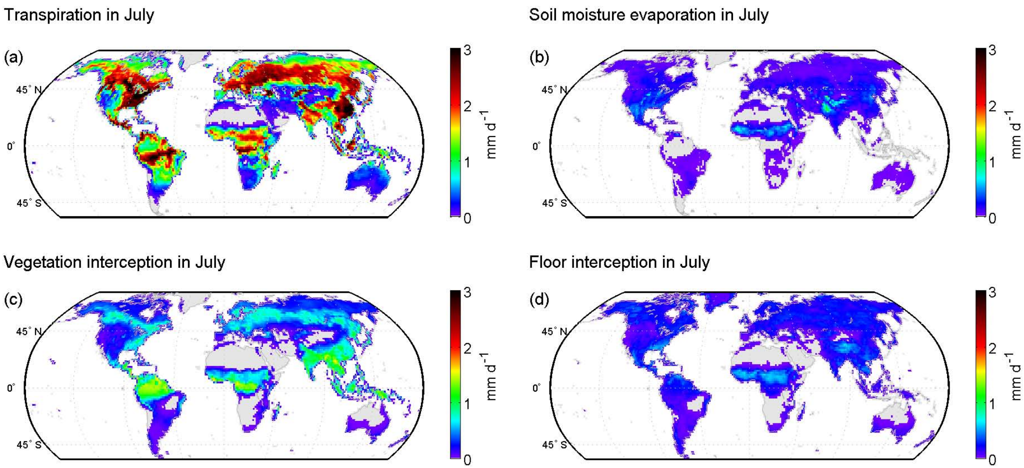

Fig. C3. Mean evaporation rates for the month of July. Grey indicates grid cells with evaporation rates below 0.01 mm d^{-1}.

ESDD
5, 203–279, 2014

Interception and transpiration – Part 1: STEAM

L. Wang-Erlandsson et al.

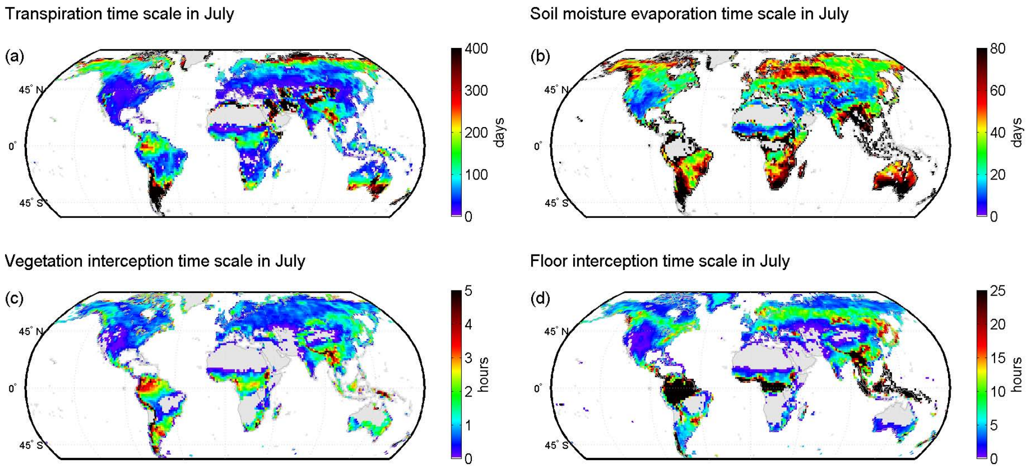

Fig. C4. Mean evaporation time scale for the month of July. Grey indicates grid cells with evaporation rates below 0.01 $mm\,d^{-1}$.

ESDD
5, 203–279, 2014

Interception and transpiration – Part 1: STEAM

L. Wang-Erlandsson et al.